REDOX REACTIVITY OF COORDINATED LIGANDS IN PENTACYANO(L)FERRATE COMPLEXES

JOSÉ A. OLABE

Departamento de Química Inorgánica, Analítica y Química Física, and INQUIMAE,
Facultad de Ciencias Exactas y Naturales, Universidad de Buenos Aires, Pabellón 2,
Ciudad Universitaria, C1428EHA, Buenos Aires, Argentina

I. Introduction

The coordination chemistry of transition metal cyanometallates has been of great and long standing concern because of the fundamental issues related to their electronic structure and reactivity. It has been

comprehensively reviewed (*1*), together with more recent developments on the solid state chemistry, comprising new synthetic and structural aspects relevant to the properties of advanced materials (*2*). Complexes containing variable relations of cyanide with other ligands in the first coordination sphere are known; however, in the present review we deal specifically with the pentacyano(L)ferrate(II) and -(III) complexes, with particular emphasis on the redox changes associated, with L. A review has been published on the basic synthetic, spectroscopic and reactivity properties of these systems (*3*). The reactivity issues comprised ligand interchange reactions (formation, dissociation, and isomerization), electron transfer and photochemical reactions, as well as some applications in dinuclear mixed-valence complexes and bioinorganics. A detailed account on the importance of high-pressure mechanistic studies for the different types of reactivity associated with the pentacyanoferrate complexes, has also been published (*4*). A more recent review reports on the advances in the chemistry of the pentacyano(L)ferrates, as well as on the ruthenium and osmium analogues, with a preliminary account of the subjects raised in this chapter (*5*). Photochemical studies have been exhaustively considered elsewhere (*4,6*), and are therefore omitted in this report. Much of the content of the present review draws heavily on the collaborative work performed by our group in recent years. This was firmly supported by the pioneering work undertaken in the 1970s by H. E. Toma, J. M. Malin and coworkers, and followed by a large number of other contributors to the field over the past two decades.

The ligands (L) binding to the $[Fe^{II}(CN)_5]^{3-}$ fragment are quite diverse (*3–5*). A key complex is $[Fe^{II}(CN)_5H_2O]^{3-}$, which can be easily prepared in solution through aquation of $Na_3[Fe(CN)_5NH_3] \cdot 3H_2O$ (*7*). The aqua-complex is an unstable species, leading to Prussian-blue type complexes as a result of the release and recombination of cyanides (*8*). It has not been isolated as a pure solid but it is an effective intermediate for binding many other L ligands, forming moderate-to-strongly stable complexes (10^3–10^6 M^{-1}) which have been well characterized in solution and generally also in the solid state (L = NH$_3$, amines, diamines, hydrazine, nitrosyl, CO, dmso, phosphines, *N*-heterocyclic ligands: py, pz and derivatives, and so forth). The complex with L = NH$_3$ can be easily prepared starting from the well known nitroprusside ion (NP), through the reaction with NH$_3$ (*7c,7d*), and it is currently used as a precursor for the preparation of other complexes, by simple substitution with the desired L ligand. Many of these Fe(II) complexes containing L ligands with low-energy LUMOs display intense metal-to-ligand charge-transfer (MLCT) absorptions in

the visible region, with the energies depending on the π-acceptor ability of L. An important advantage of the reviewed systems is the accessibility of Fe(III) complexes (*3–5*). Intense, visible-absorption bands are also shown by some of them (L = azide, thiocyanate, thiolates, etc.), suggesting a ligand-to-metal charge-transfer (LMCT) origin. These versatile spectroscopic features have been of crucial importance for the identification of products and/or intermediates in the kinetic and mechanistic studies. The redox potentials for the $[Fe^{III/II}(CN)_5L]^{2-/3-}$ couples span a range from ca. 0.4 up to 1.0 V (vs. NHE), depending on the ligand L (*3*).

Mixed-valence cyano complexes with diverse bridging ligands have been prepared. Particularly important are the "Creutz-Taube analogs", $[(NC)_5M^{II}$–pz–$M^{III}(CN)_5]^{5-}$ (pz = pyrazine; M = Fe, Ru, Os), which show remarkable changes in the electronic structure upon dissolution in different solvents (*9*). In fact, the iron mixed-valence complex appears to be a strongly localized (Class II) species in aqueous solution. It changes to a much more valence-delocalized complex in aprotic solvents such as acetonitrile, showing a borderline Class II/III behavior (*9,10*). Cyanide has also been intensively used as a bridging ligand; a vast amount of complexes of the $[(NC)_5M^{II}$–CN–$M^{III}(X)_5]^n$ series have been prepared with X = CN^-, NH_3, EDTA, polypyridines and other ancillary ligands, mainly but not exclusively with group 8 metals, showing that cyanide is a good communicating bridge for charge mediation between the metal centers. We address here only a few developments for these systems, particularly related to redox reactivity changes upon coordination of a cyano ligand through the exposed N-donor. The subject has been partially reviewed (*5*), and we suggest the interested reader to consult some specific reviews dealing with the general properties of cyano-bridged complexes, including the issue of electronic coupling and multi-electron charge transfer processes between the metal centers (*5,11*).

The present review will focus on the redox chemistry of small nitrogen-containing L ligands with bioinorganic relevance, particularly nitric oxide, NO, and its redox-interconverted forms NO^+ (nitrosyl) and NO^- (nitroside, or its protonated form, HNO, nitroxyl) (*12,13*). The ligand interchange reactions of NO will be analyzed in the context of better understanding the redox properties of the bound ligand. Both the chemically and electrochemically induced oxidation and reduction of the appropriate bound species will be considered. Comparisons between the chemistry of bound NO in NP with that found in NO–porphyrins and –chelates will be analyzed on the basis of their specific relevance to biochemical and environmental issues.

The reductive NO chemistry will cover some new developments on the electrophilic reactions of bound nitrosyl with different nucleophiles, particularly the nitrogen hydrides (hydrazine, hydroxylamine, ammonia, azide) and trioxodinitrate, along with new density functional theoretical (DFT) calculations which have allowed to better understand the detailed mechanistic features of these long-studied addition reactions, including the one with OH^-. The redox chemistry of other molecules relevant to biochemistry, such as O_2, H_2O_2 and the thiolates (SR^-) will also be presented.

The catalytic nature of some of these redox reactions will be highlighted, given the labile character of H_2O in the $[Fe^{II}(CN)_5H_2O]^{3-}$ ion. Structural and functional comparisons will be made regarding the behavior of iron-enzymes associated with the nitrogen redox cycle (*14*). Overall, the review deals mainly with the chemistry in aqueous media, with occasional mention to work in organic solvents. Cyanometallate complexes are known to display profound changes in their electronic structure and reactivity when dissolved in solvents with different acceptor capability, associated with the donor properties of the exposed electron pairs at the cyano ligands (*15*). These specific interactions are also related to the role of cationic association in the thermodynamics and kinetics of the reactions involving cyano complexes (*16*).

II. General Properties of the Nitroprusside ion, $[Fe(CN)_5NO]^{2-}$ (NP), and Related Nitrosyl Complexes

Sodium nitroprusside was first prepared and investigated in the middle of the nineteenth century, and a comprehensive summary of the earlier chemical investigations has been published (*17*). Up to 1910–1930, the addition reactions of bases to NP were explored, involving the characterization of colored intermediates (e.g., with SH^-, SR^-, and SO_3^{2-}), useful for analytical purposes. The hypotensive action of NP was first demonstrated in 1929, and a considerable research effort has attempted to establish the mode of action of NP and its metabolic fate. Questions still arise on the mechanism of NO release from NP in the biological fluids, and we refer to them below. New accounts dealing with modern structural and reactivity issues associated with the coordination of nitrosyl in NP and other complexes have appeared (*18–20*). From the bioinorganic and environmental viewpoint, nitrosyl–iron complexes have been studied with

different spectator ligands, with a recent emphasis on porphyrins (related to hemoproteins), carboxyl-binding chelates, and other biologically relevant ligands such as imidazolates and thiolates (*21,22*). According to the Enemark–Feltham notation (E–F) (*23*), the nitrosyl complexes are described as $\{MNO\}^n$, with n standing for the number of electrons associated with the metal d and π^*_{NO} orbitals. Thus, NP can be described as a member of the $\{FeNO\}^6$ class. In combination with a Walsh MO treatment, a linear FeNO structure is predicted. This electron-counting formalism considers that the $\{MNO\}$ moiety is delocalized, *avoiding the use of formal oxidation numbers* for the metal or the NO ligand. For assigning the detailed electronic distribution in the $\{MNO\}$ unit (on which the nature of the spectator ligands not included in the E–F description, may have an influence), diverse spectroscopic tools must be used (IR, EPR, Moessbauer, etc.) (*24*). Some ambiguity can remain, as shown below, and this is probably the reason for still assigning formal charges inside the $\{MNO\}$ moieties. We refer to appropriate reviews for the discussion of the electronic structure problem (*18,23*). For NP, the idealized description as $\{Fe^{II}NO^+\}$ is generally accepted, based on its geometry, diamagnetism, IR properties (high NO stretching frequency, 1918 cm^{-1}), and short Fe–N distance (1.66 Å), consistent with a strong, multiple bond. From the reactivity viewpoint, the NO$^+$ ligand is attacked by nucleophiles (see below), although it is extremely inert toward thermal dissociation, which is not detectable. Similar properties arise for other classical coordination complexes where the above description is also accepted (*25,26*). However, the reversible binding studies of NO with diverse ferri-heme proteins and complexes show very fast dissociation rates in the range of 10^3–10^7 s^{-1}, which seems to be at odds with the claimed $\{Fe^{II}NO^+\}$ formulation for $n=6$ (*25*). In fact, the best limiting description of ferri-heme nitrosyls with $n=6$ is still not clearly established. Both the low-spin $\{Fe^{II}NO^+\}$ or the antiferromagnetically coupled $\{Fe^{III}NO\}$ description have been proposed, depending on the selected spectroscopic or reactivity property under consideration (*24,27*). The $\{Fe^{II}NO^+\}$ electronic distribution is usually associated with the electrophilic reactivity, and this has been certainly observed both with classical coordination complexes and with ferri-heme compounds (*25,26,28*). On the other hand, the $\{Fe^{III}NO\}$ description seems to be more adequate for explaining the high NO-dissociation rate from the iron center in the ferri-hemes. We shall come back to this important issue.

In recent years, the photoinduced linkage isomerization reactions of bound nitrosyl appearing in different complexes have been

comprehensively studied (*19*). Pioneering studies with NP and later with other $\{MNO\}^6$ complexes (M = group 8 metals, mainly ruthenium), have shown that side-bound η^2-NO and linear η^1-ON (isonitrosyls) can be generated in situ by low-temperature laser irradiation. The characterization of the linkage isomers has been done by studying the thermal decay of the photoinduced species through differential scanning calorimetry (DSC) (*29*), as well as by IR (*30*) and Raman spectroscopies (*31*). Theoretical calculations on the ground, metastable, and excited states of NP, including the end-to-end interconversion of nitrosyl and isonitrosyl in NP have been reported (*32*). The solid-state structures have been solved by modern photocrystallographic techniques (*33*). The isomers of other small molecules (N_2, NO_2^-, SO_2) have been similarly characterized (*19*). It has been proposed (*18*) that these linkage isomers could be true intermediates on the reaction coordinate for the reversible NO-binding into the $\{FeNO\}^6$ heme-protein nitrophorin 1, existing in the saliva of some blood-sucking insects (*27*). Probably this could also be the case for the chemical and photochemical reactions associated with NO coordination and further release in NP and other nitrosyl-complexes (see below).

III. The Coordination Chemistry of NO. Formation and Dissociation Reactions

The title reactions have been insufficiently investigated. Emerging studies with iron–porphyrins and –polycarboxylic chelates (*21,22*) are directed at the significance of nitrosyl in biochemically and environ-mentally significant issues (*20*). The use of gaseous NO as a synthetic precursor to $\{MNO\}$ complexes (free of oxidizing impurities!) is contri-buting to discern on the fundamental properties of NO as a ligand, the preservation of its radical character upon coordination, and the redox interconversions leading to (formally) NO^+ or NO^- (HNO) bound spe-cies. With classical coordination compounds, the studies with pentacyano(L)ferrate(II) and -(III) systems have been very recently considered for L = NO (*34,35*). The mechanisms of ligand interchange with the $[Fe^{II/III}(CN)_5L]^{3-/2-}$ complexes have been studied for a broad range of ligands L, and have been comprehensively reviewed (*3–5*). It is generally accepted that dissociative mechanisms are operative, both for the formation and dissociation reactions. We show the case for L = NO and Fe^{II} (*34*) in reaction (1):
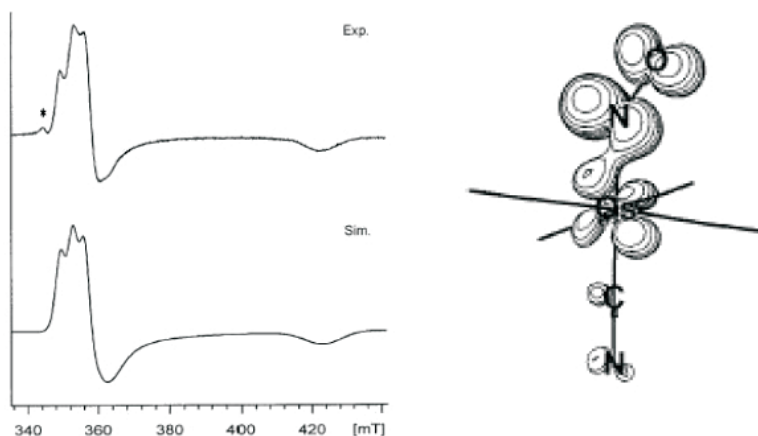
$$[Fe^{II}(CN)_5H_2O]^{3-} + NO \rightleftarrows [Fe^{II}(CN)_5NO]^{3-} + H_2O \quad k_1, k_{-1} \quad (1)$$
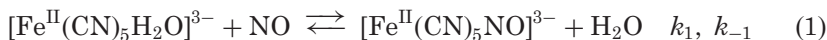
FIG. 1. (Left) Experimental and simulated EPR spectra of electrogenerated $[Os(CN)_5NO]^{3-}$ in AcN/0.1 M Bu_4NPF_6, at 3.5 K. (The asterisk denotes a low-field impurity.) (Right) Spin density distribution within $[Os(CN)_5NO]^{3-}$.

The product is a well characterized, paramagnetic {FeNO}^{7} species ($S=\frac{1}{2}$) (*36*). It can be best described as a {Fe^{II}NO$^\bullet$} unit containing a bent FeNO structure, and the EPR results and DFT calculations show that around 60% of the spin density is on the nitrosyl ligand (mainly on N), with ca. 30% remaining on iron (*37*). Figure 1 shows the experimental and simulated spectra found for the $[Os(CN)_5NO]^{3-}$ complex, together with the spin density distribution. The EPR spectral results and interpretation for the iron-derivative (*36b*) allow to propose a similar geometry and electronic distribution for the three pentacyano-complexes, which can be extended to other reduced nitrosyl-complexes containing mainly ruthenium (*26*).

The value of k_1 is 250 ± 10 M^{-1} s^{-1} (25.4 °C, $I = 0.1$ M, pH 7.0), in agreement with similar values found for the entry of many other neutral ligands into $[Fe^{II}(CN)_5H_2O]^{3-}$ (*3–5*). The activation parameters are: $\Delta H^{\#} = 70 \pm 1$ kJ mol^{-1}, $\Delta S^{\#} = +34 \pm 4$ J K^{-1} mol^{-1}, $\Delta V^{\#} = +17.4 \pm 0.3$ cm^3 mol^{-1} (*34*). These results are in agreement with a rate-controlling water release step followed by a fast coordination of NO, supporting a dissociative mechanism, most probably D (*38*). It can also be inferred that no particular influence of the unpaired electron on NO exists on the formation reaction, concluding that NO behaves as other Lewis-basic diamagnetic ligands. As to the reverse reaction in Eq. (1), the interpretation of the results is complicated by the occurrence of

reaction (2), which is an example of the general instability of $\{MNO\}^7$ complexes toward the labilization or even release of a spectator *trans*-ligand (*12,20,24*). An interesting "organic analogue" of the NO^+/NO ligand redox system was found for the mpz^+/mpz pair bound to $[Fe^{II}(CN)_5]^{3-}$ (mpz^+: *N*-methylpyrazinium ion) (*39*). The mpz-centered one-electron reduction also showed the subsequent loss of cyanide, as studied by spectroelectrochemistry and EPR techniques. The mpz^+ ligand is also a weak σ-donor as well as a strong π-acceptor, although weaker than NO^+.

$$[Fe(CN)_5NO]^{3-} \rightleftarrows [Fe(CN)_4NO]^{2-} + CN^- \quad k_2, k_{-2} \qquad (2)$$

From the values of $k_2 = 2.8 \times 10^2$ s^{-1} and $K_2 = 6.8 \times 10^{-5}$ M (*40*), it follows that $[Fe(CN)_5NO]^{3-}$ is the predominant species at pH 10. When cyanide was added to the mixture, the dissociation rate of NO from $[Fe(CN)_5NO]^{3-}$ could be measured without significant inter-ference of the tetracyano complex. Besides, cyanide also acted as a scavenger of the $[Fe^{II}(CN)_5H_2O]^{3-}$ ion in the reverse process of Eq. (1), forming $[Fe(CN)_6]^{4-}$ as a final product (*34*). In this way, the pseudo-first order decay of $[Fe(CN)_5NO]^{3-}$ allowed to obtain $k_{-1} = k_{-NO} = 1.58 \times 10^{-5}$ s^{-1} (25.0 °C, $I = 0.1$ M, pH 10.0), with $\Delta H^{\#} = 106.4 \pm 0.8$ kJ mol^{-1}, $\Delta S^{\#} = +20 \pm 2$ J K^{-1} mol^{-1} and $\Delta V^{\#} = +7.1 \pm 0.2$ cm^3 mol^{-1}. The results also agree with a dissociative mechanism, although a quan-titative interpretation of the magnitude of the activation volume waits for more available data on NO-dissociation processes in related systems.

Table I shows a comparative display of dissociation rate constants and activation parameters for a selected group of $[Fe^{II}(CN)_5L]^{n-}$ complexes. In agreement with a dissociative behavior, it can be seen that the values of k_d strongly depend on L. Although the activation enthalpies and positive entropies suggest a compensation effect, the overall picture supports the dissociative assignment (*3–5*). The value of k_{-NO} is significantly larger than for L = CN^- and CO (ca. 10^{-7}–10^{-8} s^{-1} at 25 °C) (*41,42*). It is of the same order of magnitude as for the release of other σ–π binding ligands such as dmso (*43*), pyrazine or pyridine (*44*), and much smaller than for the σ-only binding ammonia ligand (*45*). This suggests that neutral NO is a moderate σ-donor and a π-acceptor. As expected, it behaves as a stronger σ-donor although a much weaker π-acceptor than NO^+ in NP. Given the correlation between the energies of the electronic *d–d* absorption bands and the dis-sociation rate constants for L in the $[M^{II}(CN)_5L]^{n-}$ series (*46*),

TABLE I

DISSOCIATION RATE CONSTANTS AND ACTIVATION PARAMETERS FOR DIFFERENT
$[Fe(CN)_5L]^{n-}$ COMPLEXES

Ligand	k_d (s^{-1})	$\Delta H_d^{\#}$ (kJ mol^{-1})	$\Delta S_d^{\#}$ (J K^{-1} mol^{-1})	$\Delta V_d^{\#}$ (cm^3 mol^{-1})	Ref.
NO$^+$	not detected	–	–	–	
CO^b	$< 10^{-8}$				(41)
CN$^{-\ c}$	ca. 4×10^{-7}				(42)
NO	1.58×10^{-5}	106.4 ± 0.8	$+20 \pm 2$	$+7.1 \pm 0.2$	(34)
dmso	7.5×10^{-5}	110.0	$+46.0$		(43)
pz	4.2×10^{-4}	110.5	58.6	13.0	(44)
py	1.1×10^{-3}	103.8	46.0		(44)
NH$_3$	1.75×10^{-2}	102	$+68$	$+16.4$	(45)

$T = 25.0\,°C$; $I = 0.1$ M.
^{b}Estimated number, measured using pz as a scavenger.
^{c}Extrapolated from data reported at higher temperatures.

we are now able to include both NO and NO$^+$ ligands in the "spectro-chemical series" (cf. Table I). The release of NO from some five-coordinate $\{FeNO\}^7$ ferro–heme proteins (21,25) yields values of the same order of magnitude as k_{-NO} in $[Fe(CN)_5NO]^{3-}$, although impor-tant labilizing effects have been found by introducing different substi-tuents in the porphyrin ring (47). Values in the range $1–10^{-4}$ s^{-1} have been measured for the trans-$[Ru^{II}(NH_3)_4X(NO)]^{2+}$ complexes (X = H$_2$O, py, im–N, im–C, P(OEt)$_3$, etc.), as well as for trans-$[Ru(cyclam)(H_2O)(NO)]^{2+}$ (6.1×10^{-4} s^{-1}). It has been proposed that the trans effect and trans influence of the X ligand control the NO dissociation rates (26). How the rate of release of NO depends on the metal and/or the spectator ligands could be better understood by extending the work to other appropriate series.

The value of k_{-NO} in $[Fe(CN)_5NO]^{3-}$ has physiological significance, because it is believed that NO is released to the medium provided that the thiolates present in the biological fluids are able to reduce NP following injection in the blood stream in the hypertensive situa-tions (20,48). Given the fast response to this stimulation (20), k_{-NO} shows a much too small value. More probably, the competing reaction (2) is operative, allowing for final NO release through the decomposition of $[Fe(CN)_4NO]^{2-}$ (48). We refer below to this important set of reactions, related to the electrophilic reactivity of NP toward thiolates.

The coordination of NO to the $[Fe^{III}(CN)_5H_2O]^{2-}$ ion [Eq. (3)] affords a first order rate law in each reactant, with $k_3 = 0.252 \pm 0.004$ M^{-1} s^{-1}

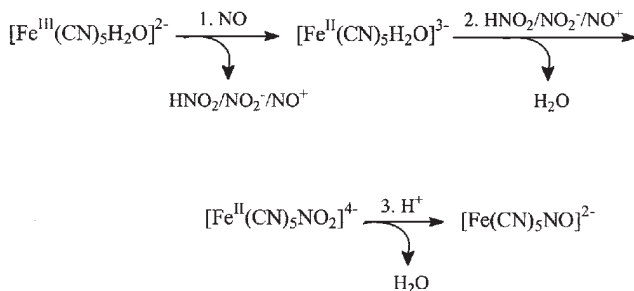$$[Fe^{III}(CN)_5H_2O]^{2-} \xrightarrow{\text{1. NO}} [Fe^{II}(CN)_5H_2O]^{3-} \xrightarrow{\text{2. } HNO_2/NO_2^-/NO^+}$$

$$\downarrow HNO_2/NO_2^-/NO^+ \qquad\qquad\qquad \downarrow H_2O$$

$$[Fe^{II}(CN)_5NO_2]^{4-} \xrightarrow{\text{3. } H^+} [Fe(CN)_5NO]^{2-}$$

$$\downarrow H_2O$$

FIG. 2. Proposed mechanism involving initial reduction of $[Fe^{III}(CN)_5H_2O]^{2-}$ by NO, forming $[Fe^{II}(CN)_5H_2O]^{3-}$, with final conversion to NP.

at 25.5 °C, $I = 0.1$ M, and activation parameters: $\Delta H^{\#} = 52 \pm 1$ kJ mol^{-1}, $\Delta S^{\#} = -82 \pm 4$ J K^{-1} mol^{-1} and $\Delta V^{\#} = -13.9 \pm 0.5$ cm^3 mol^{-1} (35). The quantitative product is NP, and k_{-3} may be considered to be zero.

$$[Fe^{III}(CN)_5H_2O]^{2-} + NO \rightleftarrows [Fe(CN)_5NO]^{2-} + H_2O \quad k_3, k_{-3} \quad (3)$$
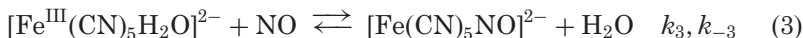
For the much slower coordination reactions of several ligands L to $[Fe^{III}(CN)_5H_2O]^{2-}$ ($k =$ ca. 10^{-4}–10^{-7} M^{-1} s^{-1}), a dissociative interchange (I_d) mechanism has been suggested (3–5,49). The data for reaction (3), particularly the negative values of the entropy and activation volume do not agree with the I_d mechanism, which predicts positive values in both cases. On the other hand, Fig. 2 describes the proposed mechanism.

The reaction involves a rate-determining reduction of Fe(III) to Fe(II) as a first step. Although an outer-sphere mechanism was proposed, the value of k_3, together with the redox potential of the NO$^+$/NO couple (1.21 V vs. NHE) (13), excludes this possibility. Instead, NO could behave as a reductant, following its association with cyanides in the precursor complex. After electron transfer, NO$^+$ is rapidly hydrolyzed to nitrite (or HNO$_2$, depending on pH), with further coordination of either of the latter species into the $[Fe^{II}(CN)_5H_2O]^{3-}$ ion, forming NP as the final product (35). Evidence for the formation of $[Fe^{II}(CN)_5H_2O]^{3-}$ as an intermediate was obtained through competition experiments in which several L ligands (pz, NCS$^-$, etc.) were used as trapping agents. Figure 3 shows the modified mechanistic scheme including the new experimental evidence. A complementary investigation of the reactivity of other $[Fe^{III}(CN)_5L]^{n-}$ complexes toward NO (L = py, pz, nitrite, cyanide) showed that NO also reacted in the

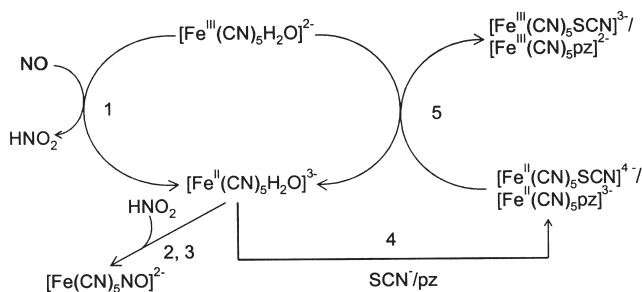FIG. 3. Mechanistic scheme for the reaction of $[Fe^{III}(CN)_5H_2O]^{2-}$ with NO, showing the competition experiments for trapping the $[Fe^{II}(CN)_5H_2O]^{3-}$ intermediate by different ligands (pz, NCS$^-$).

first step through the formation of intermediate $[Fe^{II}(CN)_5L]^{(n+1)-}$ complexes (*35*).

The above mechanistic interpretation is in contrast with the one appearing in the coordination chemistry of NO on the very labile Fe(III)–porphyrins and hemoproteins, which show water substitution-controlled kinetics at the iron(III) center (*22,25*). The latter Fe(III) moieties are, however, high-spin systems, whilst the cyano-complexes are low-spin. There is strong experimental evidence to support the dissociative mechanism with the Fe(III)–porphyrins, because the rates are of the same order as the water-exchange reactions measured in these systems (*22d*). Besides, the Fe(III) centers are less oxidizing than $[Fe^{III}(CN)_5H_2O]^{2-}$ (*21,25*).

In spite of the above mechanistic insight into the initial stages of NO coordination to the ferriheme systems, the fact is that the so-called reductive nitrosylation reaction has been observed for the water-soluble ferri-heme model Fe(III)TPPS in aqueous solution (H_2TPPS^{4-} = tetraanionic form of *meso*-tetrakis(*p*-sulfonatophenyl)porphyrin), as well as for Cyt^{III}, metMb and metHb reacting with NO at various pHs, even in slightly acidic media, pH range 6–8 (*25,50*). Figure 4 describes the proposed reaction scheme for the overall reductive nitrosylation process.

Good linear plots of the pseudo-first order rate constant for the formation of Cyt^{II} from Cyt^{III} as a function of [OH$^-$] have been found, supporting the above mechanism. Although no evidence for the N-bound nitrous acid intermediate complex was found, the k_{OH} values derived from the slopes, together with the redox potentials for nitrosyl reduction in the heme compounds are in fair agreement with the general behavior observed for the electrophilic reactions of other nitrosyl complexes, including NP (see below) (*51*).
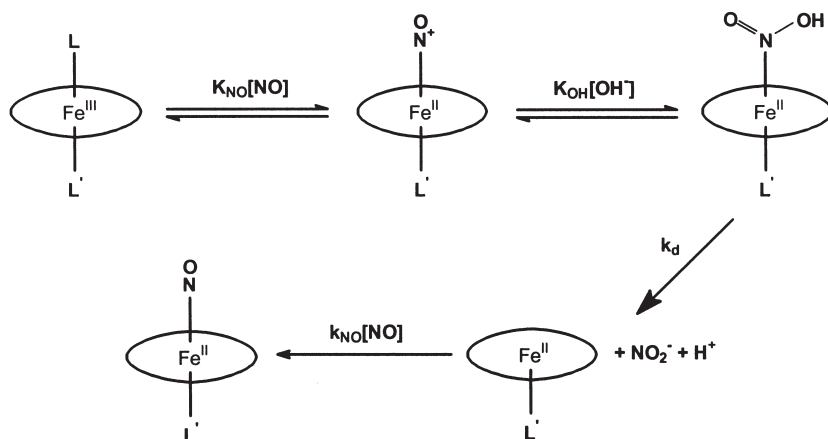
F$_{\text{IG}}$. 4. Reductive nitrosylation of ferrihemes. Proposed formation of $\{Fe^{II}NO^+\}$ as a precursor for nucleophilic attack of OH^- forming the bound nitrous acid intermediate. The release of nitrite forms a labile Fe^{II} species which binds NO forming the inert $\{Fe^{II}NO\}$ complex.

As shown in Fig. 4, a $\{Fe^{II}NO^+\}$ species has been proposed to be formed following coordination of NO into Fe(III). This reaction appears to be related to the one in Eq. (3), associated with NP formation. However, the electron-transfer step must proceed in an inner-sphere way in the Fe(III)–porphyrin system, subsequently to the water-release. As anticipated above, the evidence on the detailed electronic structure in the ferri-hemes is still ambiguous (*24,25*). Whether the species formed in the reaction of the oxidized form of heme cd_1 nitrite reductase (NiR) with NO is best formulated as $\{Fe^{II}NO^+\}$ or $\{Fe^{III}NO\}$ has been qualified as a matter of semantics (*52*) (cf. the E–F formalism), although it has been recognized that substantial donation of charge from NO to Fe(III) has occurred, supporting the $\{Fe^{II}NO^+\}$ description. The release of NO from nitrite solutions mediated by the NiR enzyme proceeds according to Eq. (4) (*14*):

$$NO_2^- + e^- + 2H^+ \xrightarrow{\text{NiR}} NO + H_2O \qquad (4)$$

The kinetics of nitrite reduction by the heme cd_1 NiR has been studied by stopped-flow (SF) and rapid-freeze EPR spectroscopy (*53*). The first step is reported to involve very fast (out of the SF time scale) binding and proton assisted dehydration of the
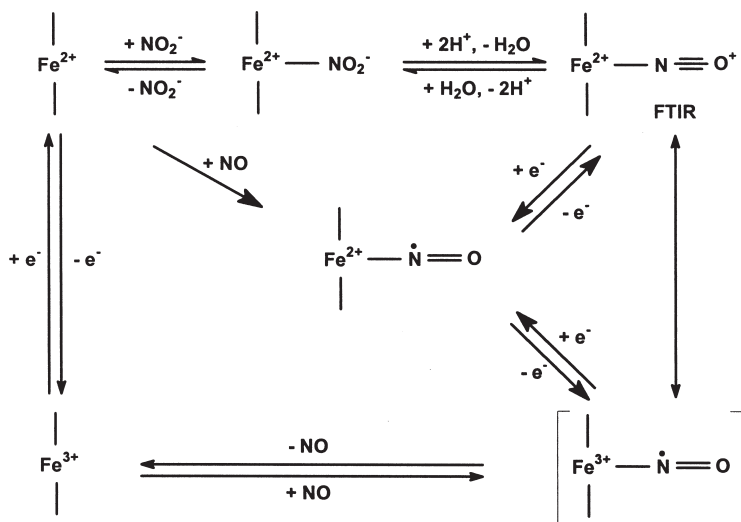
FIG. 5. Proposed mechanism for reduction of nitrite by the heme cd_1 containing nitrite reductases.

nitrite ligand to the $c^{II}d_1^{II}$ heme, resulting in the formation of a nitrosyl species, which is generally described as $\{Fe^{II}NO^+\}$. In Ref. (53), it was described as $c^{II}d_1^{III}NO$, suggesting it as the precursor of NO release. In the second step, an electron is transferred from the heme c^{II} to heme d_1^{III}, with a rate constant of 1 s^{-1} to form the paramagnetic $c^{III}d_1^{II}NO$ complex, which is rapidly reduced to $c^{II}d_1^{II}NO$ by an external reductant. On the basis of this and related work (particularly the evidence for the intermediacy of a Fe–nitrosyl species which is capable of undergoing nucleophilic attack by different nucleophiles such as water, azide, hydroxylamine) (54), Fig. 5 describes the proposed mechanism of action for the heme cd_1 NiR (14).

When oxidized NiR was put in contact with NO, the $\{Fe^{II}NO^+\}$ intermediate was directly observed by FTIR spectroscopy ($\nu_{NO}=1910$ cm^{-1}) (52). This agrees with similar values of the stretching frequency measured for related ferri-hemes (24). The high values (compared to the ferro-hemes), together with the short N–O distances (1.63–1.65 Å) are consistent with a multiple bond, and indeed support the $\{Fe^{II}NO^+\}$ description, as generally accepted for NP and other classical nitrosyl complexes.
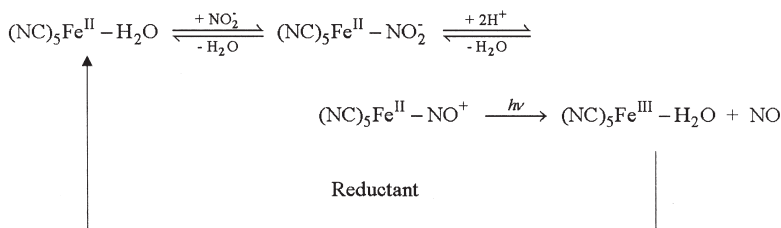
In spite of the above analysis, the remarkable fact related to the enzyme function is the ability of this $\{FeNO\}^6$ species to release NO.

The same can be said on the fast NO-release from the ferriheme compounds (*22*). It has been proposed that the heme $\{Fe^{II}NO^+\}$ moieties are highly reactive toward NO release, provided that they are not trapped by a nucleophile or reduced by one electron to the very stable Fe^{II}–NO species (*14*). We are now considering a comparison with the behavior of NP toward dissociation.

As shown above, the reverse reaction (3) was undetectable, in full agreement with the $\{Fe^{II}NO^+\}$ description. The two factors analyzed above influencing the instability of the NiR enzyme are absent for NP under normal physiological conditions. The conversion of bound NO^+ to nitrite and further release of the latter species to the medium occur at pHs higher than 10 for NP (*55*). Besides, NP can be transformed into the moderately inert $[Fe^{II}(CN)_5NO]^{3-}$ (although more labile compared to NP, see above) under reducing conditions. Then, we can postulate that NO^+ should be extremely inert toward dissociation in the different systems, unless some specific factor promoting labilization is present.

Another comparative issue between NP and the ferri-hemes emerges from the photochemical studies with NP, which have been early and successively investigated. The stoichiometry corresponds to the one observed in the reverse reaction of Eq. (3) (*6,56*). We may consider that the $\{Fe^{II}NO^+\}$ ground state in NP converts to an excited state upon irradiation, whose electronic structure is not clearly defined. It could be described as $\{Fe^{III}NO\}$, considering that the photoinduced electron transfer comprises a bonding–antibonding transition, which weakens the Fe–N bond. The fast ensuing release of NO has been quantitatively studied under different conditions, although the mechanistic details and the timing of NO release are still unknown (*6*).

The photochemical process with NP resembles the above described *thermal* one occurring in the NiR enzymes (see Eq. (4) and Fig. 5). In fact, the reduction of nitrite in the presence of $[Fe^{II}(CN)_5H_2O]^{3-}$ and the release of NO could be made photocatalytic, on the basis of the following scheme, provided that an external reductant was allowed to reduce $[Fe^{III}(CN)_5H_2O]^{2-}$ back to $[Fe^{II}(CN)_5H_2O]^{3-}$.

$$(NC)_5Fe^{II}-H_2O \underset{-H_2O}{\overset{+NO_2^-}{\rightleftharpoons}} (NC)_5Fe^{II}-NO_2^- \underset{-H_2O}{\overset{+2H^+}{\rightleftharpoons}}$$

$$(NC)_5Fe^{II}-NO^+ \overset{h\nu}{\longrightarrow} (NC)_5Fe^{III}-H_2O + NO$$

$$\text{Reductant}$$

Given that a *thermal* intramolecular redox reaction converting $\{Fe^{II}NO^+\}$ to a putative redox isomer $\{Fe^{III}NO\}$ may be rejected in NP, on the basis of the not detected NO dissociation for the reverse reaction in Eq. (3), the contrast with the heme systems becomes remarkable. Why the NiR enzyme or other ferrihemes are an exception probably relates to possible labilizing factors associated with the heme structure, as commented above for the dissociative behavior of several ferro-hemes (*47*). One could suspect that the fast release of NO in the flash-photolysis experiments with the ferri-hemes in the presence of NO could be related to the relaxation of the non-steady-state system back to equilibrium comprising the decay of an excited state species. However, studies performed in parallel using either flash-photolysis or stopped-flow techniques provided the same k_{off} values (around 30–50 s^{-1} at 25 °C) for the release of NO in experiments performed with metmyoglobin–NO mixtures (*22c*). Although a limiting Fe^{II}–NO^+ description has been adopted to ascribe the above nitrosyl complex, it is probable that the electronic structure resembles an intermediate situation between the above one and Fe^{III}–NO, or that a thermally accessible state with the latter configuration is involved in the dissociation process.

For NP, not only the dissociation rate of the formally NO^+ ligand is undetectable, but neither can the coordination of NO^+ to $[Fe^{II}(CN)_5H_2O]^{3-}$ be studied, because NO^+ is very rapidly converted to nitrite in aqueous solutions (*12,13*). Similar considerations can be raised on the coordination ability of the one-electron reduced form of NO, namely NO^- or HNO. These species are also highly reactive as precursors of N_2O in aqueous media (*13*), and therefore the formation reactions, as in Eqs. (1) and (3), cannot be studied.

IV. The Redox Reactivity of Bound NO

The one-electron electrochemical reduction of NP (*57*) is a reversible process in aqueous solution, provided the measurements are performed at pH > 8 (−0.123 V vs. NHE) (*57a,57b*). Different chemical reductants such as sodium in liquid ammonia, tetrahydroborate, ascorbic acid, quinol, dithionite, superoxide or thiolates are also known to generate the $[Fe^{II}(CN)_5NO]^{3-}$ ion (*48,57*). However, care must be taken in the products' analysis, because the negative redox potentials of some of these reductants allow for further nitrosyl reduction (*57a*). Also, the reduced product is unstable toward cyanide
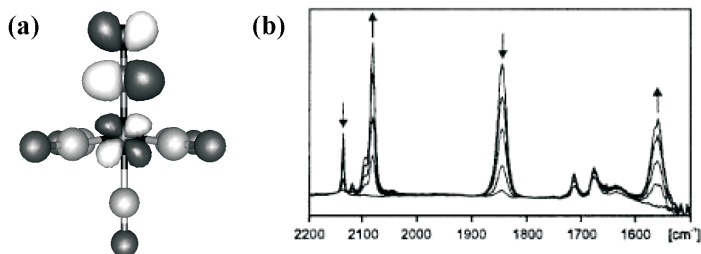
FIG. 6. (a) DFT computed LUMO of $[Fe(CN)_5NO]^{2-}$ and (b) IR–spectroelectrochemical response of $[Os(CN)_5NO]^{2-}$ on one-electron reduction in acetonitrile/ 0.1 M Bu_4NPF_6.

release [Eq. (2)], as demonstrated by pulse-radiolysis studies (40). The electrochemical evidence showed that this process can be very significant at pH < 7. A surface enhanced Raman scattering (SERS) study of the electroreduction of NP on a silver electrode in aqueous solution showed the appearance of peaks associated with the pentacyano and tetracyano reduced products (57c). The electrochemistry of NP in non-aqueous aprotic media (CH_2Cl_2 and AcN), showed that the first reduction is irreversible, with a fast conversion (< 10 ms) of the initial $[Fe^{II}(CN)_5NO]^{3-}$ product to the $[Fe(CN)_4NO]^{2-}$ ion (57d); this was identified after exhaustive electrolysis by UV–Vis and EPR spectroscopies, in agreement with the previous characterization studies (40).

The one-electron reduction of NP is associated with an increase in the population of the antibonding FeNO orbital. Figure 6a shows the DFT computed LUMO of NP (58), and Fig. 6b shows the IR electrochemical response for the $[Os^{II}(CN)_5NO]^{2-}$ ion (59) upon one-electron reduction in acetonitrile. The spectral characterization of the osmium–nitrosyl reduced complex could be done successfully because of the inertness of the Os–L bonds (L = NO or cyanide). In contrast, NP rapidly releases a cyanide ligand upon reduction in acetonitrile (57b,57d). The strong decrease of both the v_{CN} and v_{NO} stretching frequencies in $[Os^{II}(CN)_5NO]^{3-}$ is very noticeable, particularly v_{NO}. This is as predicted from the LUMOs description, since the addition of electrons to $[Os^{II}(CN)_5NO]^{2-}$ must weaken the NO bond.

An alternative description of the one electron reduced product of NP was earlier associated with the protonation of nitrosyl (20,57a). Further electrochemical studies discarded the onset of this species in the overall electroreduction of NP (57e). The results of
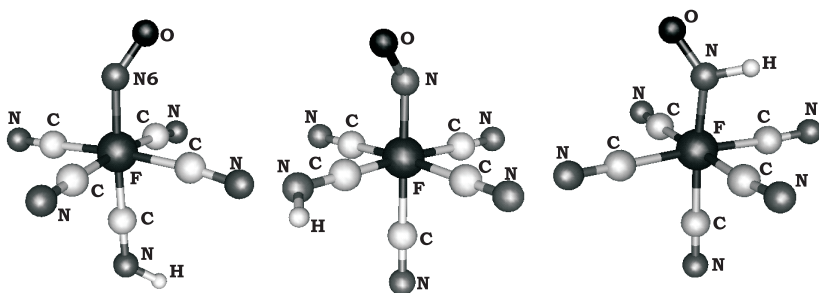
FIG. 7. Optimized geometries of the most stable cyano-protonated complexes of $[Fe(CN)_5NO]^{3-}$ and $[Fe(CN)_5HNO]^{3-}$.

the DFT calculations in Fig. 7 showed unstable structures for the nitrosyl-protonated species (58). In contrast, protonation of cyanides is feasible. It is now evident that both experimental and theoretical results support $[Fe^{II}(CN)_5NO]^{3-}$ as a stable form of the one electron reduction product of NP. Cyanide protonation should be operative only for pHs lower than 3, as found for related $[Fe^{II}(CN)_5L]^{3-}$ complexes (44).

The $[Fe^{II}(CN)_5NO]^{3-}$ ion can be oxidized back to NP in the presence of oxygen (see the reactions of NP with thiolates below) (57,60). Detailed kinetic studies on this important bioinorganic oxidation reaction are not available. In a more general context, the mechanism of the autoxidation reactions of NO complexes awaits a systematic study, which could in principle be afforded with the known $\{MX_5(NO^+)\}$ series (M = Fe, Ru or Os; X = amines, polypyridines, etc.), if appropriate reductants were used to generate the NO complexes.

The electrochemical processes occurring with NP at more negative potentials with respect to the first reduction wave are strongly pH-dependent, and are also influenced by the concentration ratio $[H^+]/[NP]$. The second one-electron wave has been associated with the reduction of the $[Fe(CN)_4NO]^{2-}$ ion, both in acidic and alkaline media (57a,57e), discarding the early proposed reduction of $[Fe(CN)_5NOH]^{3-}$ in the acidic range (57a). It has been proposed that $[Fe(CN)_4NO]^{2-}$ evolves in different ways upon reduction at pHs 7.6 and 3.0, according to studies by square-wave (SW) and cyclic voltammetry (CV), with the consumption of one and three electrons, respectively (57e). The $[Fe(CN)_4NO]^{2-}$ ion generates the Hg-adsorbed

$[Fe(CN)_4NO]^{3-}$ ion upon one-electron reduction, followed by a proton-induced disproportionation reaction to regenerate $[Fe(CN)_4 NO]^{2-}$, along with the formation of $[Fe(CN)_4NH_2OH]^{2-}$. The overall reaction involves a four-electron reduction of NP to the hydroxylamine complex.

On the other hand, upon electrolysis under conditions of a two-electron reduction of NP at pH 8.8, a product has been detected with an absorption band at 445 nm, but there is no conclusive evidence on its structure (*57a*). Thus, the expected, highly elusive product HNO has not yet been adequately characterized in the pentacyanoferrate systems. However, recent DFT calculations on $[Fe^{II}(CN)_5HNO]^{3-}$ have been reported, affording a stable species with a defined geometry and spectroscopic properties (*58*). Figure 7 shows that protonation of nitrosyl at the nitrogen atom is operative for the two electron reduced product of NO, as expected for a highly nucleophilic $\{Fe^{II}NO^-\}$ moiety; on the other hand, the unprotonated species containing the nitroside (NO^-) anion was found to be unstable. The calculated values for the ν_{CN} and ν_{NO} stretching frequencies showed a decreasing trend when going successively from NP to the one-electron and two-electron reduced products. Particularly, the ν_{NO} values 1932, 1650, and ca. 1350 cm^{-1}, respectively, agree with an increasing population of the Fe–NO antibonding LUMO. A consistent increase in the NO bond length was calculated to be 1.16, 1.20, and 1.25 Å, respectively, and this is accompanied by the decrease of the FeNO angle: 177, 147, and 138 degrees, respectively. Both geometrical features agree with the predictions of the E–F formalism. The calculated values for the distance and angle for $[Fe^{II}(CN)_5HNO]^{3-}$ are in excellent agreement with experimental data reported for HNO in well characterized complexes, as revealed by structural and spectroscopic results for several inert, octahedral ruthenium and osmium centers. Different synthetic strategies for obtaining HNO complexes afforded either the selective oxidation of bound hydroxylamine, or the hydride reduction of NO complexes (*61*).

The HNO ligand in $[Fe^{II}(CN)_5HNO]^{3-}$ appears to be a very reactive species, precluding its direct spectroscopic characterization, as done for the Ru and Os complexes (*61*). However, supporting chemical evidence on the transient existence of $[Fe^{II}(CN)_5HNO]^{3-}$ has been provided during the reduction of NP with 1,2-dimethylhydrazine (*62*), as well as in the oxidation reaction of hydroxylamine to NP (*63*). This is discussed below. Although HNO should be expectedly labile toward dissociation from the iron center on the time scale of minutes (using a comparative estimation based on the dissociation rate of

NO from $[Fe^{II}(CN)_5NO]^{3-}$, see above), it seems that this time period is sufficient for HNO to survive long, before being attacked by external redox reagents, or affording a dimerization process leading to N_2O. In fact, the reactivity issues related to the bound HNO ligand have not been clearly disclosed yet, even for the well characterized Ru and Os complexes ([61]).

The irreversible electroreduction of NO^+ in NP, past the two-electron reduction stage, yields bound hydroxylamine, involving a four-electron process. Some ambiguity still exists, as to the presence of five or four cyanide spectator ligands ([51a,e]). On the other hand, the chemical reduction with 1,2-dimethylhydrazine affords a complete six-electron reduction to ammonia ([62]). Ammonia is also produced in the electrocatalytic reduction of nitrite with the water-soluble $[Fe^{III}(H_2O)$ $(TPPS)]^{3-}$ ion ([64]), as well as in the reactions of some assimilatory and dissimilatory NiR enzymes ([14]). The stabilization of Fe–HNO and Fe–NH_2OH intermediates on the route to NH_3 has been postulated for both the electrochemical ([64]) and the enzymatic ([65]) processes. In the latter case, the evidence comes from the crystallographic information on cytochrome c NiR and from DFT calculations on the detailed mechanism of the six-electron process, which also considers the initial key $NO_2^- \rightarrow NO^+$ conversion at the Fe(II) site. From the previously described and from older studies on nitrosyl reductions ([66]), we conclude that the nature of the reduction products of NO^+ strongly depends on the reductant, the nitrosyl complex and the medium conditions, making the consideration of a systematic behavior difficult. See below, however, information on the reactions of hydrazine and substituted derivatives with bound NO^+ ([62]).

V. The Electrophilic Reactions of Bound NO

The electrophilic reactions of the nitrosyl ligand constitute one of its most important reactivity modes ([12,13,25]). This has been known for a long time, and comprehensive reviews are available ([28]). A general way of describing the course of the reactions of NP with different nucleophiles is through Eqs. (5) and (6):

$$[Fe^{II}(CN)_5NO]^{2-} + B \rightleftarrows \{[Fe^{II}(CN)_5NO \cdot B\}^{n-} \qquad (5)$$

$$\{[Fe^{II}(CN)_5NO \cdot B\}^{n-} + OH^- \rightleftarrows [Fe^{II}(CN)_5H_2O]^{3-} + products \qquad (6)$$
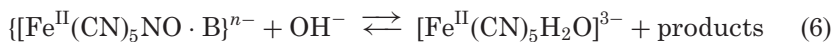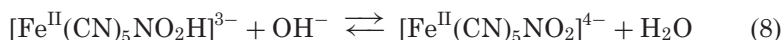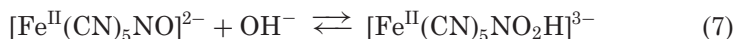
Equations (5) and (6) are supported by solid evidence for the overall stoichiometries and the general way the reaction rates increase with the concentration of OH^-. This is also valid for related complexes of the $[MX_5NO]^n$ series ($M = Fe^{II}$, Ru^{II}, Os^{II}, Ir^{III}; $X =$ amines, polypyridines, etc.). The nucleophiles B bind to the N atom of NO, and can be very diverse: OH^-, N-binding species (NH_3, amines, hydrazine, hydroxylamine, azide, trioxodinitrate), S-binding ones (SH^-, thiolates, sulfite), organic molecules, etc. The reactions occur for nitrosyl complexes bearing formal $\{M^{II}NO^+\}$ electronic distributions, for which high NO-stretching frequencies (> 1860 cm^{-1}) are usually found (*28*).

With the exception of $B = OH^-$, which relates in fact to an acid–base reaction, the other nucleophiles are potential reductants. After forming the reversible adducts [Eq. (5)], redox reactions are usually operative, leading to the reduction of nitrosyl and oxidation of the nucleophile in Eq. (6). Nevertheless, we will consider first the reaction with $B = OH^-$ for the sake of simplicity, and also because it allows for some generalizations to be made on the factors that influence the electrophilic reactivities of different nitrosyl complexes (*51*). We continue with new results for some N-binding nucleophiles (*62,67*), which throw light on the mecanisms of N_2O/N_2 production and release from the iron centers. A description of the state of the art studies on the reactions with thiolate reactants as nucleophiles will be presented later.

A. Reactivity of Nitrosyl Complexes with OH^-

The reaction scheme can be described as:

$$[Fe^{II}(CN)_5NO]^{2-} + OH^- \rightleftarrows [Fe^{II}(CN)_5NO_2H]^{3-} \qquad (7)$$

$$[Fe^{II}(CN)_5NO_2H]^{3-} + OH^- \rightleftarrows [Fe^{II}(CN)_5NO_2]^{4-} + H_2O \qquad (8)$$

The rate law for NP and other nitrosyl complexes approaches a first order behavior in each reactant for most of the studied systems, affording high values of $K_{eq} = K_7 \times K_8$, and sufficiently high concentrations of OH^- (*55,68*). The final product has been clearly identified as $[Fe^{II}(CN)_5NO_2]^{4-}$. No direct spectroscopic evidence on the intermediacy of $[Fe^{II}(CN)_5NO_2H]^{3-}$ has been obtained, although kinetic evidence has been provided (*55b*). A mechanistic interpretation consistent with the value of the second order rate constant and

$\Delta E=0.123$ a.u.

TS
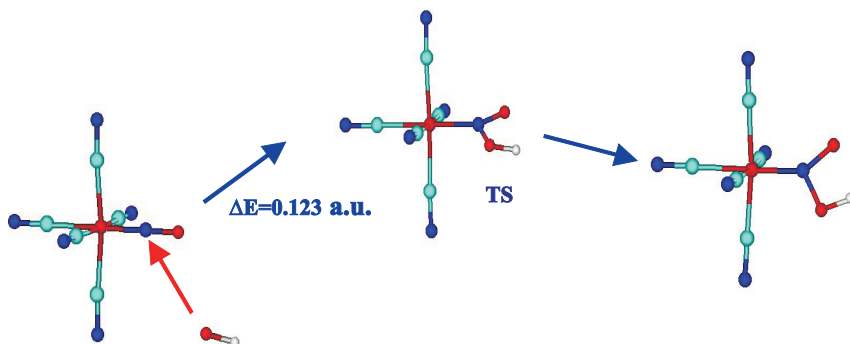
FIG. 8. Optimized geometries for the initial steps of the reaction of NP with OH^- giving the TS and the nitrous acid intermediate.

activation parameters proposes a reversible adduct formation and decay of the intermediate, with k_{OH} being the specific rate constant for OH^- addition in the first (forward) step of Eq. (7) (cf. also Eq. (5)). This mechanism has been generally accepted, and supporting evidence was obtained from DFT calculations, allowing for the structural and electronic characteristics of the different complexes along the reaction coordinate (51). Figure 8 shows the optimized geometries for the adduct-formation step, showing the conversion of linear FeNO into the angular Fe–NO$_2$H intermediate, including the description of the transition state (TS).

The energy required on going from NP to the TS is largely associated with the electronic reorganization of the N atom, while the energy involved in the evolution from the TS to the intermediate adduct is mainly associated with the change in hybridization of the O atom, from sp^3 in the OH^- ion to sp^2 in the coordinated adduct. The calculations show an increase in the bond lengths on the FeNO moiety (Fe–N and N–O) for $[Fe^{II}(CN)_5NO_2H]^{3-}$, as well as those associated with the cyano fragment, compared to NP, suggesting an increase in the electron population of the antibonding system (Table II). The angles decrease from a linear to an angular geometry, and the IR stretching frequencies decrease accordingly when going to the intermediate and final product.

In spite of the abundant work on this type of reactivity, no rate constants for the addition reactions had been obtained, with the exception of the $[M(CN)_5NO]^{2-}$ ions (M = Fe,Ru,Os) (55,68), until the recently published kinetic measurements for a representative set of nitrosyl complexes $\{MX_5NO\}^n$ (M = mainly ruthenium) (51). Table III

TABLE II

SELECTED DISTANCES (Å), ANGLES (DEGREES), AND IR STRETCHING FREQUENCIES (ν, cm^{-1}) CALCULATED FOR THE DIFFERENT STEPS OF REACTION 1, AT THE B3LYP/ 6-31G** LEVEL

	$[XNO]^{2-}(exp)^a$	$[XNO]^{2-}$	TS[b]	$[XNO_2H]^{3-}$	$[XNO_2]^{4-}$
d_{FeC} ax	1.9257(9)	1.9694	1.9878	1.9888	1.987
d_{FeC} eq^c	1.935	1.9595	1.9890	1.9880	2.011
d_{FeN}	1.6656(7)	1.6155	1.8223	1.813	2.104
d_{CN} ax	1.1591(12)	1.1683	1.1751	1.1755	1.184
d_{CN} eq^c	1.1613	1.1691	1.1761	1.1782	1.1826
d_{NO}	1.1331(10)	1.1604	1.2255	1.2275	1.2642
d_{NO}(H)			1.4536	1.4713	1.2642
d_{OH}			0.9801	0.9784	
∡ FeNO	176.03(7)	179.96	134.69	133.11	122.48
∡ ONO			109.25	107.98	115.02
∡ CFeC eq^d	176.63(4)	180.00		173.5	179.83
ν_{CN}(s)	2147–2177	2161–2170		2100–2120	2043
ν_{NO}(s)	1943	1907		1567, 1266, 789	1317, 1351, 802
ν_{Fe-N}(s)	658	712		575	574

Experimental values are given where available. X = [Fe(CN)$_5$].

[a]Ref. (33).

[b]Transition state.

[c]The fourth digit averaged.

[d]Backward the NO$_2$H group.

shows the addition rate constants, together with potential indicators of NO^+ reactivity, such as the redox potential, $E_{NO+/NO}$, and the infrared NO stretching frequency, ν_{NO}.

Figure 9 shows a linear-free-energy-relationship (LFER), revealing a very good linear correlation of the addition rate constants with the redox potentials for reactions similar to Eq. (7) with different complexes containing several MX$_5$ fragments (the complexes with [Ru(py)$_4$X] fragments stand in a parallel line, with slower rates than predicted by the main line, due to possible steric constraints upon addition of OH$^-$). The correlation is much better than the one obtained by using the NO stretching frequencies. Figure 9 shows that the rates increase with the potential, reflecting the different bonding interactions afforded by the spectator ligands. Figure 10 shows that the increase in rate constants and redox potentials parallels an increase in *both* the activation enthalpies and entropies.

The trends in the entropies are associated with the different solvational changes related to the reactions of species carrying equal or opposite charges. The reactions of the positively charged complexes

TABLE III

ADDITION RATE CONSTANTS, ACTIVATION PARAMETERS AND CORRESPONDING ν_{NO}, $E_{NO^+/NO}$ AND K_{eq} VALUES FOR DIFFERENT $\{MX_5NO\}^n$

Compound	k_{OH} (M^{-1}s^{-1})[a]	k_3 (s^{-1})[b]	$\Delta H^{\#}$ (kJ/mol)	$\Delta S^{\#}$ (J/Kmol)	$E_{NO^+/NO}$ (V)[c]	ν_{NO} (cm^{-1})[c]	K_{eq} (M^{-2})[d]
(1) cis-[Ru(AcN)(bipy)$_2$NO]$^{3+}$	$(5.60 \pm 0.07) \cdot 10^6$	$2.31 \cdot 10^6$			0.35	1960	
(2) cis-[Ru(bipy)(terpy)NO]$^{3+}$	$(3.17 \pm 0.02) \cdot 10^5$	$1.31 \cdot 10^5$	89 ± 1	159 ± 5	0.25	1946	$2.1 \cdot 10^{23}$
(3) cis-[Ru(bipy)$_2$(NO$_2$)NO]$^{2+}$	$(5.06 \pm 0.02) \cdot 10^4$	$2.75 \cdot 10^4$	83 ± 7	120 ± 20	0.18	1942	
(4) cis-[Ru(bipy)$_2$ClNO]$^{2+}$	$(8.5 \pm 0.1) \cdot 10^3$	$4.6 \cdot 10^3$	100 ± 3	164 ± 8	0.05	1933	$1.6 \cdot 10^{15}$
(5) trans-[NCRu(py)$_4$CNRu(py)$_4$NO]$^{3+}$	$(9.2 \pm 0.2) \cdot 10^3$	$3.4 \cdot 10^3$	91 ± 4	135 ± 10	0.22	1917	$3.2 \cdot 10^{15}$
(6) trans-[RuClNO(py)$_4$]$^{2+}$	$(4.6 \pm 0.3) \cdot 10^1$	$3.1 \cdot 10^1$	62 ± 1	-6 ± 5	0.09	1910	
(7) trans-[Ru(NCS)NO(py)$_4$]$^{2+}$	$(2.03 \pm 0.01) \cdot 10^2$	$1.36 \cdot 10^2$			0.12	1902	
(8) trans-[Ru(OH)NO(py)$_4$]$^{2+}$	$(2.4 \pm 0.1) \cdot 10^{-1}$	$1.6 \cdot 10^{-1}$			-0.22	1866	
(9) trans-[Ru(NH$_3$)$_4$NO(pz)]$^{3+}$	$(1.77 \pm 0.04) \cdot 10^2$	$9.55 \cdot 10^2$	76 ± 2	54 ± 6	-0.11	1942	$6.0 \cdot 10^8$
(10) trans-[Ru(NH$_3$)$_4$(nic)NO]$^{3+}$	$(3.3 \pm 0.1) \cdot 10^1$	$1.8 \cdot 10^1$	78 ± 1	44 ± 4	-0.18	1940	$5.9 \cdot 10^7$
(11) trans-[Ru(Clpy)(NH$_3$)$_4$NO]$^{3+}$	$(2.60 \pm 0.05) \cdot 10^1$	$1.40 \cdot 10^1$			-0.19	1927	$6.0 \cdot 10^6$
(12) trans-[Ru(NH$_3$)$_4$NO(py)]$^{3+}$	$(1.45 \pm 0.02) \cdot 10^1$	$7.82 \cdot 10^0$			-0.22	1931	$2.2 \cdot 10^5$
(13) trans-[Ru(4-Mepy)(NH$_3$)$_4$NO]$^{3+}$	$(9.54 \pm 0.06) \cdot 10^0$	$5.14 \cdot 10^0$	75 ± 1	26 ± 4	-0.25	1934	$7.7 \cdot 10^5$
(14) trans-[Ru(hist)(NH$_3$)$_4$NO]$^{3+}$	$(7.6 \pm 0.4) \cdot 10^{-1}$	$4.12 \cdot 10^{-1}$			-0.39	1921	$4.6 \cdot 10^1$
(15) [Fe(CN)$_5$NO]$^{2-}$	$5.5 \cdot 10^{-1}$ [8d]	$3.9 \cdot 10^0$	53 [8d]	-49 [8d]	-0.29 [15]	1945 [8d]	$1.5 \cdot 10^5$
(16) [Ru(CN)$_5$NO]$^{2-}$	$9.5 \cdot 10^{-1}$ [8d]	$6.4 \cdot 10^0$	57 [8d]	-54 [8d]	-0.35 [15]	1926 [8d]	$4.4 \cdot 10^6$
(17) [Os(CN)$_5$NO]$^{2-}$	$1.37 \cdot 10^{-4}$ [8d]	$8.63 \cdot 10^{-4}$	80 [8d]	-73 [8d]	-0.68 [15]	1897 [8d]	$4.2 \cdot 10^1$

[a]Derived from the rate-law.
[b]Obtained through $k_3 = k_{OH}/K_{ip}$, with K_{ip} being estimated according to an electrostatic model.
[c]Ref. (51).
[d]See Ref. (51) for the corresponding citations in the literature.
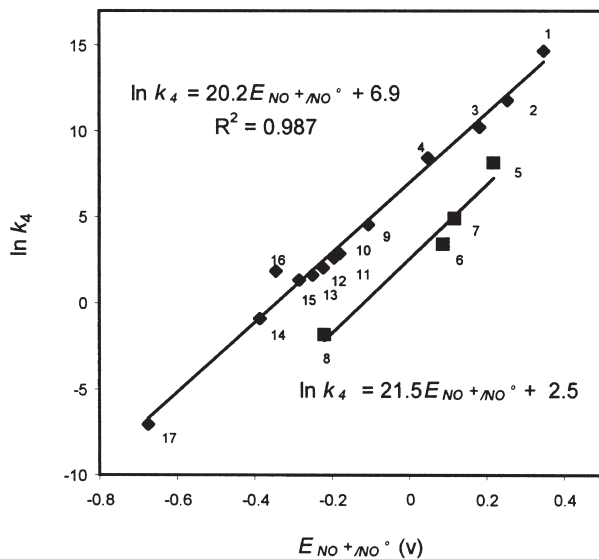
F$_{\text{IG}}$. 9. LFER plot of $\ln k_4$ (addition rate constant) vs. $E_{\text{NO}+/\text{NO}}$ for the reactions of a series of $\{MX_5NO\}^n$ complexes with OH^-. See Table III for the assignment of numbers.
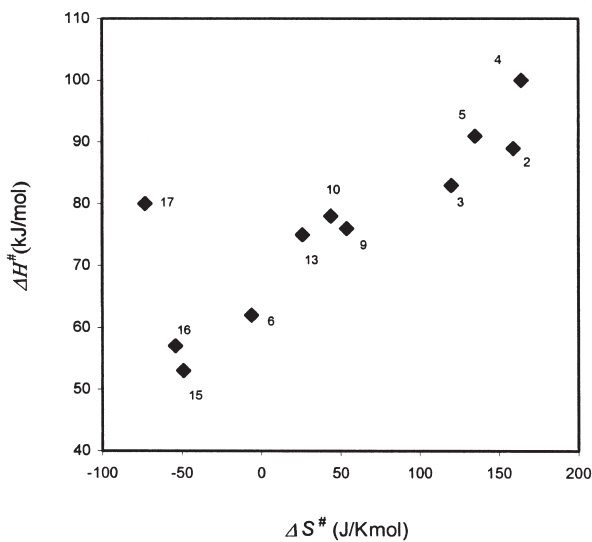

F$_{\text{IG}}$. 10. Plot of the activation enthalpies versus the activation entropies for the reactions of $\{MX_5NO\}$ complexes with OH^- (see Table III).

with OH^- are expected to favor an increase in entropy because of charge neutralization, and the opposite effects are expected with the reactions of the negatively charged complexes. On the other hand, the increase in enthalpy associated with an increase in rate is not so obvious. It was proposed that the enthalpy change should be controlled mainly by the energetically costly steps involving the reorganization of the linear MNO to angular MNO_2H in the TS (see above). This cost will be maximal for the complexes at the top of Table II, associated with a larger triple bond character of the NO bond. For a selected group of complexes in Table II, other descriptors of the electrophilic reactivity have been calculated, namely the charge on the delocalized center, q_{MNO}, as well as the energy of the LUMO (*51*). The first ones are shown in Table IV. The DFT calculations also allowed for the optimized geometries of the reactants and intermediates for a selected group of complexes included in the table, as shown in Fig. 11. These also showed similar elongated bonds and smaller MNO angles for the intermediates compared to the reactants, as already discussed for NP.

Table III also shows the values of the equilibrium constants, K_{eq}, for the conversion of iron–nitrosyl complexes into the corresponding nitro derivatives. K_{eq} decreases downwards, meaning that the conversions are obtained at a lower pH for the complexes at the top of the table. Thus, NP can be fully converted into the nitro complex only at pHs greater than 10. The $NO^+-NO_2^-$ conversion, together with the release of NO_2^- from the coordination sphere, are key features in some enzymatic reactions leading to oxidation of nitrogen hydrides to nitrite (*14*). The above conversion and release must occur under physiological conditions with the hydroxylaminoreductase enzyme (HAO), in which the substrate is seemingly oxidized through two electron paths involving HNO and NO^+ as intermediates. Evidently, the mechanistic requirements are closely related to the structure of the heme sites in HAO (*69*). No direct evidence of bound nitrite intermediates has been reported, however, and this was also the case for the reductive nitrosylation processes associated with ferri-heme chemistry (Fig. 4) (*25*).

Recently, it has been shown that NP and its ruthenium and osmium analogs engage in dinuclear complex formation with the $[Ru(NH_3)_5H_2O]^{2+}$ ion (*70*). In all cases, a new intense, broad absorption is displayed in the visible region, which is not present in either of the reacting chromophores. By proposing a $[(NH_3)_5Ru^{II}-NC-M(CN)_4NO]$ structure (M = Fe, Ru, Os), it was suggested that the intense band was associated with a donor–acceptor charge transfer (DACT)

TABLE IV

STRUCTURAL AND ELECTRONIC PARAMETERS DERIVED FROM CALCULATIONS USING PSEUDOPOTENTIALS FOR THE METAL CENTERS[a]

		d_{M-N}	d_{N-O}	$d_{N-O(H)}$	$\angle MNO$	$\angle ONO$	q_N	q_{NO}	q_{MNO}	ν_{NO}
$[Ru(AcN)(bpy)_2NO]^{3+}$	LAN	1.806	1.134		178.2		0.128	0.138	1.148	1993
	SDD	1.778	1.137		178.6		0.207	0.127	1.112	1981
$[Ru(AcN)(bpy)_2NO_2H]^{2+}$	SDD	1.994	1.203	1.389	128.0	114.2				
$[Ru(bpy)(trpy)NO]^{3+}$	LAN	1.799	1.137		175.3		0.108	0.101	1.131	1974
	SDD	1.772	1.141		176.2		0.176	0.082	1.115	1964
$[Ru(bpy)(trpy)NO_2H]^{2+}$	SDD	1.991	1.204	1.391	128.4	114.3				
$[Ru(bpy)_2ClNO]^{2+}$	LAN	1.786	1.139		172.7		0.136	0.106	0.779	1969
	SDD	1.759	1.143		175.5		0.182	0.058	0.779	1959
$[Ru(bpy)_2ClNO_2H]^{+}$	SDD	1.965	1.207	1.405		114.4				
$[RuA_4NO(py)]^{3+\,b}$	LAN	1.825	1.129		180.0		0.165	0.094	0.847	2005
	SDD	1.792	1.133		180.0		0.213	0.081	0.899	1983
$[RuA_4NO_2H(py)]^{2+\,b}$	SDD	1.952	1.209	1.394	128.6	114.7				
$[Ru(CN)_5NO]^{2-}$	LAN	1.779	1.163		180.0		0.004	−0.215	−0.067	1874
	SDD	1.758	1.164		180.0		0.105	−0.201	−0.169	1871
$[Ru(CN)_5NO_2H]^{3-}$	SDD	1.969	1.225	1.464	133.1	108.7				
$[Fe(CN)_5NO]^{2-}$	LAN	1.618	1.157		180.0		0.222	−0.026	−0.576	1906
	SDD	1.617	1.158		180.0		0.197	−0.063	−1.327	1901
$[Fe(CN)_5NO_2H]^{3-}$	SDD	1.833	1.224	1.457	132.9	108.6				

[a]Distances (d) in Å; angles in degrees; q_N: calculated charge on the N atom of the NO group; q_{NO}: calculated charge on the NO group, q_{MNO}; calculated group-charge. See Ref. (51) for details.
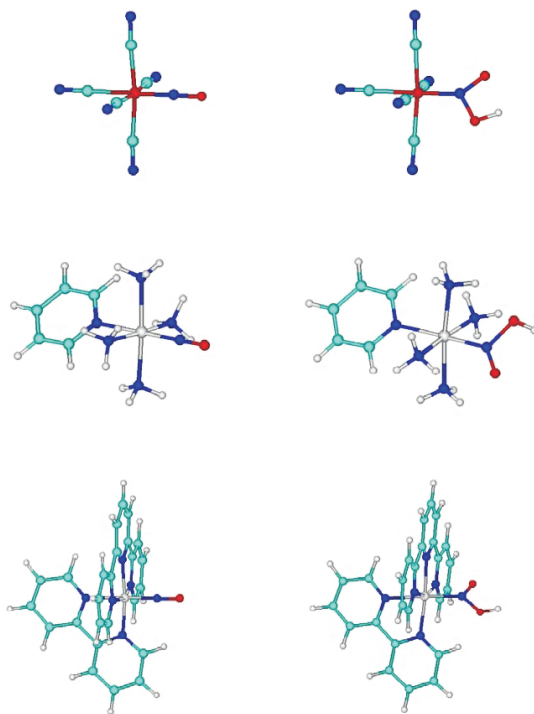
[b]A = amine.

FIG. 11. Optimized geometries at the B3LYP/6-31G** level (SDD pseudopotentials on the metal centers) for representative members of the set (nitrosyls and OH$^-$ addition products): (a) [Fe(CN)$_5$NO]$^{2-}$; (b) *trans*-[Ru(NH$_3$)$_4$NO(py)]$^{3+}$; (c) *cis*-[Ru(bpy)(trpy)NO]$^{3+}$.

interaction between the remote Ru(II) center and the delocalized {MNO} moiety. The absorption features resemble the properties of mixed-valence, cyano-bridged complexes with {M^{III}X$_5$} acceptor fragments (X = cyanides, ammonia, etc.) (*71*), although in the new situation the acceptor is not metal-centered, but is associated with the delocalized {MNO}. Although a crystal structure was not obtained (thus, the *cis*- or *trans*-character of NO with respect to the bridging cyanide is uncertain), IR-Raman, UV–Vis and electrochemical studies were performed, showing significant changes in the relevant absorption energies upon potential-controlled redox changes leading to oxidation of the ruthenium center or reduction at the nitrosyl site. Most important from the reactivity point of view considered in this review, was the fact that the rate constant for the nucleophilic addition of OH$^-$ to the bound nitrosyl was enhanced by ca. five orders

of magnitude when the remote Ru(II) was oxidized to Ru(III). This long distance effect is indeed associated with the good electronic communication ability of bridging cyanide (*5*). The previous kinetic study was performed in a preliminary way for M = Os, but it is likely that a similar rate increase should occur for the iron- and ruthenium analogs. A better characterized dinuclear complex, *trans*-[NC(py)$_4$Ru^{II}–CN–Ru(py)$_4$NO]$^{3+}$ was prepared later, showing similar spectroscopic and kinetic results (*72*). The latter species is attractive because of the possibility of building trinuclear (or polynuclear) species through coordination of other fragments to the exposed cyanide ligand, thus allowing for systematic studies of structure–reactivity correlations in extended linear arrays.

B. Reactivity of NP with Hydrazine (Hz), MeHz, and 1,1-Me$_2$Hz

Surprisingly, among the variable set of nucleophiles whose reactions had been studied with NP, the case of N_2H_4 was absent, in contrast with data available for some ruthenium–nitrosyl complexes (*28*).

Recent work describes the addition reactions of hydrazine and substituted derivatives to NP (*62*). The kinetic studies were done using UV–Vis absorption and mass spectrometric methods. Different stoichiometries were found, depending on the nucleophile. We can distinguish three different mechanistic paths, and these will be successively presented, with an effort to extract some common mechanistic features.

It was proposed that the initial step is a reversible adduct formation comprising the N-atom of the nucleophile and the N-atom of the delocalized {FeNO} moiety (which we identify as Fe^{15}NO), as described in Eq. (9).

$$[Fe^{II}(CN)_5^{15}NO]^{2-} + NHR_3NR_1R_2 \rightleftarrows [Fe(CN)_5^{15}N(OH)NR_3NR_1R_2]^{2-}$$

$$(9)$$
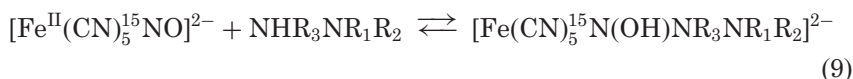
This reaction has been written in a generalized manner; the R_i substituents are H or Me, depending on the nucleophile under consideration. Although no details of the adduct structures can be obtained through the kinetic measurements, a deprotonation of the binding N-atom of the nucleophile is assumed. As a second key hypothesis, if another H-atom is bound to the central N ($R_3 = H$) in Eq. (9), it should be reactive toward OH$^-$. Further proton transfer and electronic

reorganization consummate the reaction. Thus, Eq. (9) is followed by Eq. (10):

$$[Fe(CN)_5^{15}N(OH)NR_3NR_1R_2]^{2-} + OH^- \longrightarrow [Fe(CN)_5H_2O]^{3-}$$
$$+ N^{15}NO + NHR_1R_2 \tag{10}$$
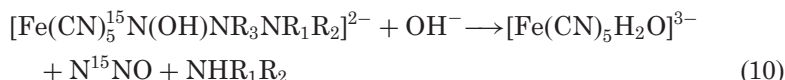
Equations (9) and (10) describe the reaction of Hz ($R_1 = R_2 = H$), giving NH_3 as a product. They can also be used for MeHz in one of its reactive modes, predominant at pHs below 7 ($R_1 = H$, $R_2 = Me$), rendering $MeNH_2$ as a product and, finally, for 1,1-Me_2Hz in its main reactive mode ($R_1 = R_2 = Me$), giving this time Me_2NH as a product. Equation (11) describes the overall stoichiometry for this main path, taking Hz as the nucleophile:

$$[Fe^{II}(CN)_5NO]^{2-} + N_2H_4 + OH^- \longrightarrow [Fe^{II}(CN)_5H_2O]^{3-} + NH_3 + N_2O \tag{11}$$
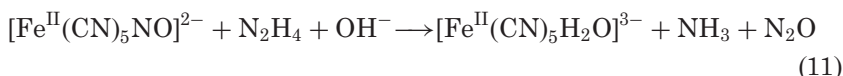
These reactions were studied in excess of hydrazine, and were pseudo-first order in complex. At constant pH, the plots of the rate constants (s^{-1}) against the concentration of hydrazine were linear, allowing for the calculation of the second-order rate constant, $k_{N2H4} = 0.43$ M^{-1} s^{-1} (25 °C, pH 10), with $\Delta H^{\#} = 26.8 \pm 0.2$ kJ mol^{-1}, $\Delta S^{\#} = -163 \pm 5$ J K^{-1} mol^{-1}. The plot of k_{N2H4} against pH (Fig. 12, which includes data for the substituted hydrazines as well) showed an apparent first-order dependence with respect to OH^- in the low pH limit and zero order at high pH. The pH-dependence accounts for the role of OH^- in Eq. (10). By applying the steady-state treatment to the adduct species in Eqs. (9) and (10), an expression was derived having the same form as the experimental rate law as shown in Fig. 12.

The proposed mechanism agrees with the general picture presented in Eqs. (5) and (6). The electronic reorganization of the adduct allows the release of N_2O and NH_3, with $[Fe^{II}(CN)_5H_2O]^{3-}$ formation [Eq. (11)]. Strong evidence for the mechanism was obtained by using ^{15}N in NP, with the result that the label appeared only in $N^{15}NO$, as measured by mass spectrometry, but not in NH_3 or in the amines.

The formation of $[Fe^{II}(CN)_5H_2O]^{3-}$ as a product sets the basis for the catalytic processing of nitrite reduction by hydrazine under appropriate pH conditions. As shown in Fig. 13, nitrite binds to the aqua ion and rapidly converts to NO^+. After the attack by N_2H_4, the adduct reorganization, associated with proton migration steps, favor
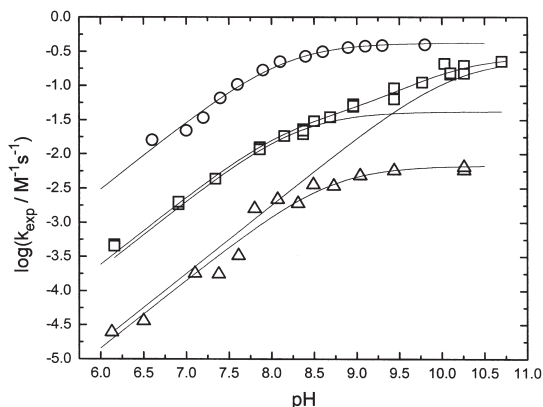
FIG. 12. Dependence of log k_{exp} on pH for the reaction of $[Fe(CN)_5NO]^{2-}$ with hydrazines. Upper curve: Hz; intermediate curve: MeHz; lower curve: 1,1-Me$_2$Hz. $T = 25.0\,°C$, $I = 0.1$ M. For MeHz, the broken lines represent the individual contributions of each term in the rate equation (*62*).
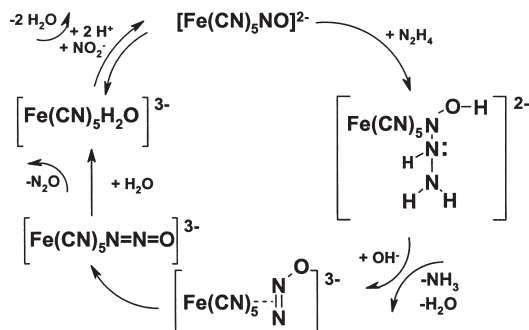
FIG. 13. Catalytic cycle showing the nucleophilic atack of hydrazine on NP, with adduct formation and reorganization. Ammonia is released, with formation of bound N$_2$O-linkage isomers. The release of N$_2$O generates the active site, $[Fe(CN)_5H_2O]^{3-}$, which coordinates nitrite, with rapid conversion to bound NO$^+$ in NP.

the cleavage of the N–N bond in hydrazine, with release of NH$_3$ and formation of bound N$_2$O.

Figure 13 illustrates the novel result of N$_2$O formation, isomerization and release, as predicted by the theoretical calculations. Figure 14a shows a DFT study (B3LYP) of the reaction profile [Eq. (11)], allowing to characterize intermediates on the potential hypersurface. It can be seen that the initially formed η^2-N$_2$O complex isomerizes to the linear
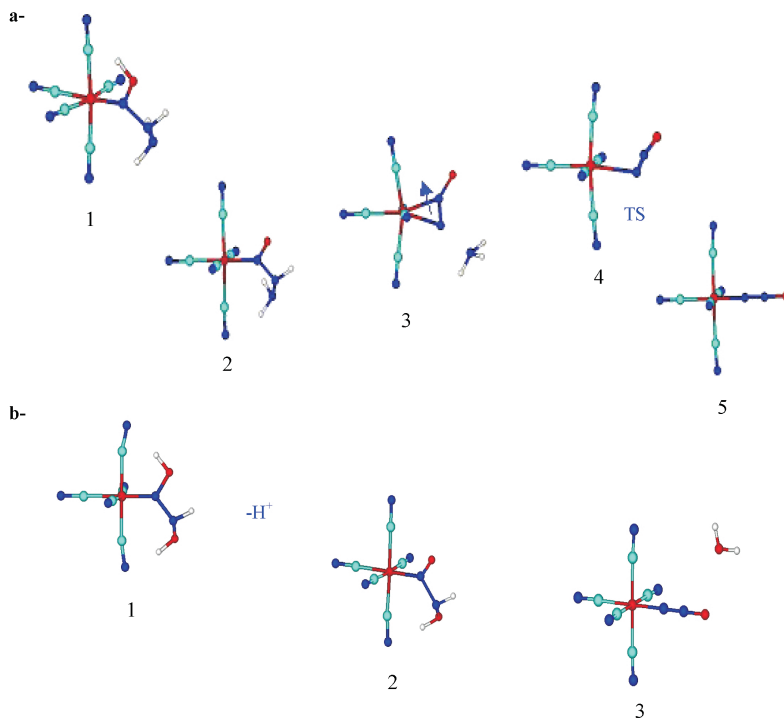
FIG. 14. (a) Schematic representation of the initial steps involved in the reaction of $[Fe(CN)_5NO]^{2-}$ with hydrazine, rendering the N_2O-bound intermediates. The structures correspond to single points on the potential hypersurface, calculated at the B3LYP/6-31G** level. Relative energies (y-coordinate) are not drawn to scale. Arrows indicate changes in the molecule that lead to the next step. From left to right: 1: $[(NC)_5FeN(OH)NHNH_2]^{2-}$; 2: $[(NC)_5FeN(O)NHNH_2]^{3-}$; 3: $[(NC)_5Fe-\eta^2-N_2O]^{3-}$; 4: TS structure; 5: $[(NC)_5Fe-\eta^1-N_2O]^{3-}$; (b) The same for hydroxylamine. From left to right: 1: $[(NC)_5FeN(OH)NHOH]^{2-}$; 2: $[(NC)_5FeN(O)NHOH]^{3-}$; 3: $[(NC)_5Fe-\eta^1-N_2O]^{3-}$.

η^1-N_2O complex, followed by release of N_2O to the medium. The mechanism of hydrazine addition in the first steps of the addition process are entirely similar as previously described for OH^- as a nucleophile, referring to the geometrical and bond distance changes, as shown in Table V.

Besides the remarkable results associated with the N_2O-isomers (62), the mechanism of reaction (11) has several additional interesting features: (1) The products are different, compared to the reactions

TABLE V

Calculated Distances (Å), Angles (deg), and Selected IR Frequencies (cm^{-1}) for the Reactant, $[Fe(CN)_5NO]^{2-}$ (NP), and the Deprotonated Adduct Intermediates, $\{Fe(CN)_5NO \cdot B\}^{n-}$, Formed by Reaction with Nucleophile B, for B $= N_2H_4$, NH_2OH, NH_3, and N_3^-

	FeNO (NP)	FeNO–N_2H_4	FeNO–NH_2OH	FeNO–NH_3	FeNO–N_3^-
Fe–N	1.615	1.785	1.787	1.789	1.825
N–O	1.160	1.376	1.377	1.367	1.443
N–N$_1$[a]	–	1.365	1.385	1.354	1.310
N$_1$–N$_2$[b,c]		1.405	1.403	–	1.342
Fe–C *cis*	1.959	1.962	1.955	1.960	1.983
trans	1.965	1.972	1.958	1.960	1.971
C–N *cis*	1.169	1.172	1.175	1.173	1.175
trans	1.168	1.172	1.170	1.169	1.175
∢ FeNO	179.9	123.0	124.8	125.6	121.3
∢ FeNN$_1$		133.0	130.8	129.0	133.9
∢ NN$_1$N$_2$[c]		115.8	114.5	–	109.7
ν_{NOH}[d]		1008, 1041	1006, 1487	989	906
ν_{NNH}[d]		1021, 1160, 1310	751, 1414	819, 1188	1090
ν_{CN}	2160	2127–2172	2125–2176	2122–2172	2130–2143

[a]N$_1$: N atom binding to nitrosyl.

[b]N$_2$: N atom binding to N$_1$.

[c]N$_2$ is O for the case of NH$_2$OH.

[d]H must be replaced by N for the cyclic azide intermediate.

of hydrazine with other nitrosyl complexes, $[Ru^{II}(NH_3)_5NO]^{3+}$ and $[M^{II}(pdma)_2Cl(NO)]^{2+}$ (M = Ru, Os; pdma: *o*-phenylenebis(dimethy-larsine)), which lead to $HN_3 + H_2O$, as apparent precursors of N_2O and N_2 (although not NH_3) (*28*). Evidently, the adduct decomposition modes depend on the nature of the MX_5 fragment in the original nitrosyl-complexes, and this is an issue which merits further study. (2) It shows a rare example of N_2O formation (it has been also found in the related electrophilic reactions of HNO_2) as a product of hydrazine oxidations, which generally lead to N_2 (*73*). (3) The formation of NH_3 as a product generated by a two-electron oxidant is also a novel feature in the mechanistic redox chemistry of hydrazine (*73*). (4) The catalytic cycle for nitrite reduction shows some similarities with the above described chemistry of dissi-milatory NiR enzymes (*14*), in the sense that the latter are also able to process nucleophiles such as hydrazine (*54*); however, a crucial difference is that N_2O, but not NO is released as a reduction

product of nitrite bound as NP, with the interesting detail that neither NO nor NO^- (or HNO) are detectable intermediates. The direct production of N_2O has also been observed for some fungal denitrifications (*14*).

An alternative reaction path was found for MeHz, as shown in Eq. (12).

$$2[Fe^{II}(CN)_5{}^{15}NO]^{2-} + MeHNNH_2 + 2OH^-$$
$$\longrightarrow 2[Fe^{II}(CN)_5H_2O]^{3-} + N^{15}N + N^{15}NO + MeOH \qquad (12)$$

$$[Fe^{II}(CN)_5{}^{15}NO]^{2-} + MeHNNH_2 + OH^-$$
$$\longrightarrow [Fe^{II}(CN)_5H_2O]^{3-} + MeNH_2 + N^{15}NO \qquad (11')$$
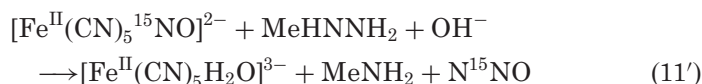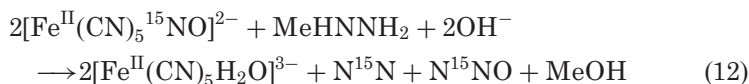
The different distribution of products in Eq. (12) compared to the main path [Eq. (11′)] was evident at pHs greater than 8. The mass balance accounted for 0.7 mol of N_2O and 0.3 mol of N_2 and MeOH, per mole of initial NP, and the labeling experiments showed that ^{15}N was distributed among $N^{15}N$ and $N^{15}NO$, of molar masses 29 and 45, respectively, supporting the simultaneous occurrence of Eqs. (12) and (11′), which is equivalent to Eq. (11) previously used for Hz. Therefore, MeHz is able to attack the nitrosyl group by two parallel paths, either using the N atom close to the Me group or the other one. The spectral results showed that a shoulder developed at ca. 480 nm (in addition to the characteristic maximum of $[Fe^{II}(CN)_5MeHz]^{3-}$ at 400 nm), suggesting a mixture of complexes. The intensity of this shoulder increased with the progress of the reaction, with no further decay after 80–90% of initial NP was transformed into $[Fe^{II}(CN)_5MeHz]^{3-}$. The new path in Eq. (12) was traced to adduct formation through the methylated N-atom of MeHz. As the adduct intermediate has no reactive H at the central N-atom, OH^- may then react as in Eq. (13):

$$[Fe(CN)_5{}^{15}N(OH)NMeNH_2]^{2-} + OH^-$$
$$\longrightarrow [Fe(CN)_5N(OH)NMeNH]^{3-} + H_2O \qquad (13)$$
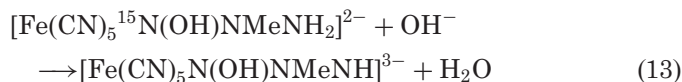
The product of Eq. (13) is probably responsible for the persistent absorbance at 480 nm. The deprotonated adduct may react as a nucleophile toward another NP, giving a dimer which, induced

by OH^- attack, may further rearrange by cleavage at the unlabeled N–N bond and displacement of the Me group, Eq. (14).

$$[Fe(CN)_5{}^{15}N(OH)NMeN^{15}N(OH)Fe(CN)_5]^{5-} + OH^- + H_2O$$
$$\longrightarrow 2[Fe^{II}(CN)_5H_2O]^{3-} + N^{15}N + N^{15}NO + MeOH \qquad (14)$$
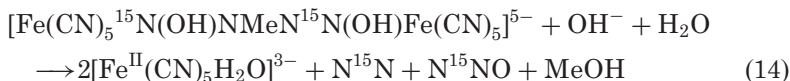
The reaction with 1,1-Me_2Hz showed a similar alternative path; however, the existence of two methyl groups on the nucleophilic N-at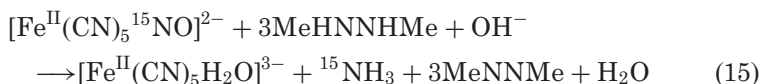om made this contribution negligibly slow. On the other hand, 1,2-Me_2Hz showed a completely different mechanism, which is described below (62).

C. REACTIVITY OF NP WITH 1,2-Me_2Hz

The new stoichiometry was as follows:

$$[Fe^{II}(CN)_5{}^{15}NO]^{2-} + 3MeHNNHMe + OH^-$$
$$\longrightarrow [Fe^{II}(CN)_5H_2O]^{3-} + {}^{15}NH_3 + 3MeNNMe + H_2O \qquad (15)$$

The formation of azomethane as a two-electron oxidation product of 1,2-Me_2Hz, and the exclusive label on $^{15}NH_3$ suggest that the full six-electron reduction of NO^+ to NH_3 is accomplished through three successive two-electron processes. The plausible intermediates must be $[Fe^{II}(CN)_5{}^{15}HNO]^{3-}$ and $[Fe^{II}(CN)_5{}^{15}NH_2OH]^{3-}$. The proposed mechanism involves an initial adduct formation, similar as for other hydrazines (the DFT calculations show that the adduct formation is not sterically hindered), as shown by Eq. (16), followed by a two-electron transfer from 1,2-Me_2Hz to the N-atom in nitrosyl, Eq. (17).

$$[Fe(CN)_5{}^{15}NO]^{2-} + MeHNNHMe \rightleftharpoons [Fe(CN)_5{}^{15}N(OH)NMeNHMe]^{2-}$$
$$(16)$$

$$[Fe(CN)_5{}^{15}N(OH)NMeNHMe]^{2-} + OH^-$$
$$\longrightarrow [Fe^{II}(CN)_5H^{15}NO]^{3-} + MeNNMe + H_2O \qquad (17)$$
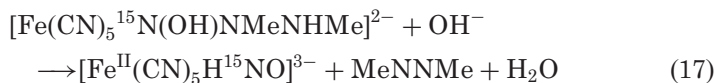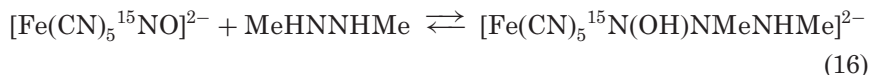
It can be seen that the formation of N_2O through the cleavage of the N–N bond, as occurring for other hydrazines, is avoided. The nucleophile is able to form a very stable product, azomethane, by transferring two electrons and protons. Thus, the nitroxyl species, $[Fe^{II}(CN)_5 H^{15}NO]^{3-}$, can be formed in Eq. (17) and survive enough to react with

another 1,2-Me$_2$Hz, forming another intermediate, [Fe^{II}(CN)$_5$^{15}NH$_2$OH]$^{3-}$ [Eq. (18)] which has been described in the literature, although its identity could be questioned (74). Its transient existence is however very likely, as suggested in the electrochemical reduction process of iron–nitrosyl-porphyrins (64). The final two-electron reduction in Eq. (19) leads to [Fe^{II}(CN)$_5$NH$_3$]$^{3-}$, which rapidly releases NH$_3$ to the medium.

$$[Fe^{II}(CN)_5H^{15}NO]^{3-} + MeHNNHMe$$
$$\longrightarrow [Fe^{II}(CN)_5{}^{15}NH_2OH]^{3-} + MeNNMe \qquad (18)$$

$$[Fe^{II}(CN)_5{}^{15}NH_2OH]^{3-} + MeHNNHMe$$
$$\longrightarrow [Fe^{II}(CN)_5{}^{15}NH_3]^{3-} + MeNNMe + H_2O \qquad (19)$$
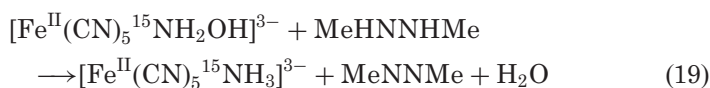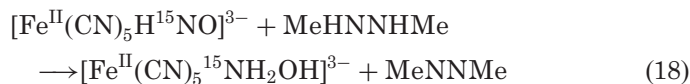
If the analyzed mechanistic possibilities were not considered as diverse and (interestingly) complicated, showing the influence of the hydrazine substituents on the reaction path, the last reaction of NP with 1,2-Me$_2$Hz also showed an alternative reaction mode, leading to the same products as in Eq. (15), although with formation of the intermediate complex [Fe^{II}(CN)$_5$NO]$^{3-}$. This was detected by EPR. It was proposed that 1,2-Me$_2$Hz added to two NP reactants, thus transferring one electron to each NP (62).

Figure 15 shows a mechanistic description of the addition of 1,2-Me$_2$Hz to NP, leading to a catalytic behavior in the presence of excess nitrite. The new feature of the catalytic reaction, compared to the stoichiometric process described by Eq. (15), is that no NH$_3$ is produced but, instead, N$_2$O is evolved (azomethane is the other product in both cases, however). The left-hand cycle describes this behavior. It was assumed that nitrite traps the [Fe^{II}(CN)$_5$NH$_2$OH]$^{3-}$ intermediate forming N$_2$O, as already studied independently in the reaction of NP with NH$_2$OH (75, see below). The right hand cycle shows the participation of the radical [Fe^{II}(CN)$_5$NO]$^{3-}$ ion in the alternative route which finally leads to the same products as in the main reaction path. Under stoichiometric conditions, when no excess of nitrite is present in the medium, the [Fe^{II}(CN)$_5$NH$_2$OH]$^{3-}$ intermediate can be further reduced to [Fe^{II}(CN)$_5$NH$_3$]$^{3-}$ [Eq. (19)].

We refer to the original work (62) in order to further analyze the above results. Summarizing, the key mechanistic requirements in the addition behavior of hydrazine and its substituted derivatives are the presence of two protons in an adjacent position to the reacting N atom for the evolution of fast addition processes leading to cleavage
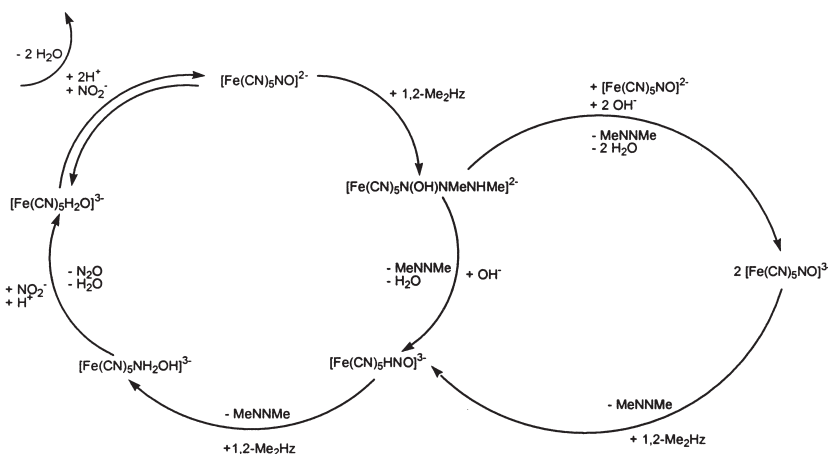
FIG. 15. Catalytic mechanism for the addition of 1,2–Me_2Hz to $[Fe(CN)_5NO]^{2-}$ in excess of nitrite, showing the participation of $[Fe(CN)_5NO]^{3-}$ in an alternative path.

of the N–N bond, as described in Eq. (11). If one Me substituent is present at the attacking position in place of H, an alternative route is developed through dimer formation and evolution of mixtures of N_2/N_2O, together with the production of MeOH (see above, Eq. (12)). With 1,1-Me_2Hz, the addition through the bis-methylated N-atom is disfavored with respect to the main path; some adduct is formed, however, but no gaseous products are released. The case of 1,2-Me_2Hz in Eq. (15) is a peculiar situation related to the specific structure of the reactant; thus, the N–N cleavage is avoided, and, instead, a stable N=N bond is formed in azomethane. As a brief conclusion of the pattern of reactions obtained with NP reacting with the structurally related hydrazine-derivatives as nucleophiles, $1e^-$, $2e^-$, and $6e^-$ paths have been found, depending on the reductant, with intermediates appearing at the $2e^-$ and $4e^-$ stages for the full $6e^-$ process. In each case, kinetic control is revealed for the corresponding reaction profiles and the different intermediates and products consequently formed.

D. REACTIVITY OF NP WITH OTHER NITROGEN HYDRIDES: NH_2OH, NH_3, AND N_3^-

These reactions have been comprehensively studied in the literature (75,76). Given the mechanistic similarities with the addition

reactions of other nucleophiles, and the success of the DFT metho-
dology in establishing the geometries of the reactants, intermediates
and products for the above discussed reactions with OH^- and N_2H_4, a
similar study was afforded for reactions (20–22) (67). The stoichiome-
tries of the relevant reactions are as follows:

$$[Fe^{II}(CN)_5NO]^{2-} + NH_2OH + OH^- \longrightarrow [Fe^{II}(CN)_5H_2O]^{3-} + N_2O + H_2O \tag{20}$$

$$[Fe^{II}(CN)_5NO]^{2-} + NH_3 + OH^- \longrightarrow [Fe^{II}(CN)_5H_2O]^{3-} + N_2 + H_2O \tag{21}$$

$$[Fe^{II}(CN)_5NO]^{2-} + N_3^- + H_2O \longrightarrow [Fe^{II}(CN)_5H_2O]^{3-} + N_2 + N_2O \tag{22}$$
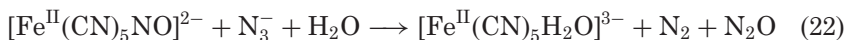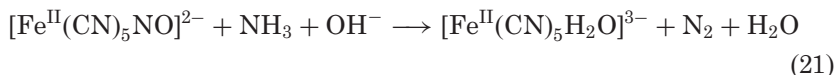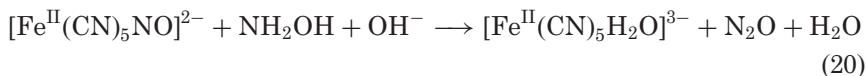
All of these reactions are assumed to proceed through the general
pattern described by Eqs. (5) and (6). Experimental results and mecha-
nistic analysis led to the following values for the forward nucleophilic
rate constants in Eq. (5), associated with reactions (20–22): $k_{NH2OH} =$
4.6 (pH 9, 26 °C, $I = 1$ M) (75), $k_{N_3^-} = 0.2$ (23 °C, $I = 1$ M) (75). Ammonia is
a poor nucleophile toward NP in aqueous alkaline solutions (76). An
estimation of k_{NH3}, ca. 10^{-4}–10^{-5} M^{-1} s^{-1} (50 °C) (76b) showed it to be
much lower than the one for OH^-, $k = 0.55$ M^{-1} s^{-1} (25 °C, $I = 1$ M) (55).
Significantly higher values of k_5 have been measured for the more
polarizable sulfur binding nucleophiles, ca. 10^2–10^4 M^{-1} s^{-1} (77).
The differences in the values of k_5 still allow to include most of the
studied electrophilic reactions of nitrosyl in a common mechanistic
framework, as described by Eqs. (5) and (6).

Figure 14b shows the calculated geometries for the hydroxylamine-
adduct, rendering the η^1-N_2O complex.

Table V summarizes the relevant calculated distances, angles, and
IR frequencies for the different adducts, including the one with
hydrazine. Again, the linear-to-bent transformation of the FeNO
moiety can be observed, as with OH^-, and an elongation of the Fe–N
and N–O distances occurs, showing the decrease in bond order. The
bending agrees with the E–F rules, in the sense that the addition
process involves a two-electron transfer to the antibonding LUMO,
forming a $\{FeNO\}^8$ species. The LUMO is highly delocalized in the
FeNO moiety, with mainly π^*_{NO} character (18,23).

By displaying the η^1-N_2O complex, Fig. 14b shows a significant
contrast with Fig. 14a, where the η^2-N_2O isomer was formed first, with
ensuing conversion to η^1-N_2O. In Fig. 14a, linear η^1-N_2O is not easily

attained in a single step from the initial hydrazine-adduct, since it is η^2-N_2O that only needs angular reorganization after release of NH_3. Also, the TS for the conversion lies higher in energy, as expected. The η^1-isomer is the more stable form, and this is understandable, given the existence of the well characterized $[Ru(NH_3)_5(\eta^1\text{-}N_2O)]^{2+}$ (*78*). The structure and reactivity of the pentaammine-L and penta-cyano-L complexes show close similarities (*79*), although the greater lability of L in the latter ones is well recognized (*3,5*).

It is a remarkable fact that the mechanisms of adduct decompositions differ significantly for the hydrazine and hydroxylamine complexes. In the hydrazine-adduct, the oxygen atom of the resulting N_2O is obviously the one previously existing in NP [Eq. (9)]. With hydroxylamine, however, the labeling experiments have demonstrated that the O-atom in N_2O comes from this reactant (*75*). The O atom belonging to NO is released as water, leaving the linear intermediate, after angular reorganization, in a single step. The main structures involved, shown in Fig. 14, are true minima in the potential hypersurface. In this case, the proposed mechanism is substantially supported by the experimental evidence. The different kinetic stabilization of the intermediates offers an explanation for this crucial mechanistic feature that differentiates nucleophiles that are structurally as similar as hydrazine and hydroxylamine.

Figure 16 shows the DFT results for reaction (21). Figure 16a shows the structure of the calculated adduct-intermediate and of the η^1-N_2 isomer that is attained by its further conversion.

The formation of N_2 can be described as a comproportionation reaction, with a three-electron interchange between the reactants and further proton and OH^- loss. The end-on linear coordination mode, η^1-N_2, is well known to be a stable form for N_2 bound to transition metal centers (*80*).

In addition, Fig. 16b shows that a stable energy minimum can also be obtained for the η^2-N_2 intermediate. The η^1-N_2 isomer was calculated to be more stable by 1.06 eV than the η^2-N_2 one. For the reaction shown in Fig. 16b, the energy of the adduct is lower than that of η^2-N_2, and therefore the intermediate is not expected to occur. Note however that the η^2-N_2 mode has been observed in low-temperature irradiated samples of $[Os(NH_3)_5(\eta^1\text{-}N_2)][PF_6]_2$ (*81*). The DFT calculated distances, angles, and IR frequencies for the η^1-N_2 linkage isomer are in agreement with reported values for related N_2-complexes, and the values for the η^2-N_2 isomer also agree with those measured for the osmium complex analogue, as shown in Table VI. As to the calculated values for the $[Fe(CN)_5N_2O]^{3-}$ isomers, given that they have not
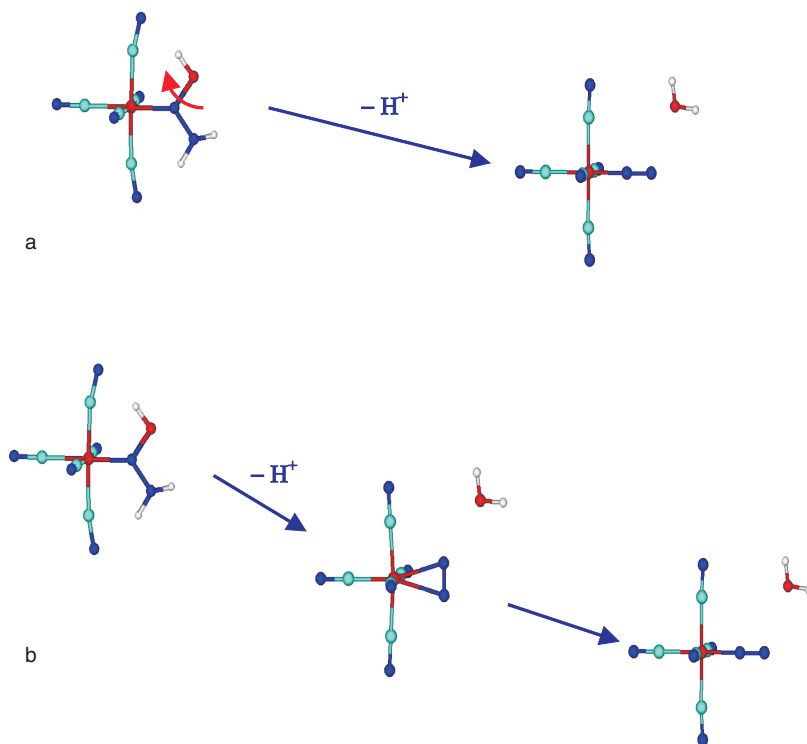
FIG. 16. Structures involved in the decomposition of the adduct intermediate resulting from the reaction of $[Fe(CN)_5NO]^{2-}$ with NH_3. (a) Only the formation of the linear, η^1-N_2 complex is considered. (b) The formation of η^2-N_2 as an intermediate step is also included. The structures correspond to single points on the potential hypersurface, calculated at the B3LYP/6-31G** level. Relative energies are not drawn to scale. Arrows indicate changes in the molecule that lead to the next step.

been described in the literature, we have compared them with IR data for the $[Ru(NH_3)_5(\eta^1\text{-}N_2O)]^{2+}$ ion and with the bond distances in free N_2O (78). No structural data exists for any type of N_2O coordination compounds.

Finally, Fig. 17 shows the geometry of the cyclic adduct formed by azide with NP, together with the calculated decomposition paths, with different possible intermediates (see Eq. (22)). Although the cyclic structure has been predicted for related metallonitrosyl adducts (82), this was not the case for the reaction with NP, where a

TABLE VI

CALCULATED DISTANCES (Å), ANGLES (deg) AND RELEVANT IR FREQUENCIES (cm^{-1}) FOR THE STABLE INTERMEDIATES FORMED WITH N$_2$O AND N$_2$ LIGANDS AFTER THE DECOMPOSITION OF THE DIFFERENT ADDUCTS DESCRIBED IN THE TEXT

	η^2-N$_2$O[a,b]	η^1-N$_2$O[a,b]	η^2-N$_2$[c,d]	η^1-N$_2$[c,d]
Fe–N	2.075, 1.992	1.820	2.226, 2.226	1.793
N–O	1.254	1.242	–	–
N–N	1.191	1.138	1.133	1.128
Fe–C *cis*	1.975	1.990	1.988	1.989
trans	1.949	1.962	1.928	1.976
C–N *cis*	1.175	1.176	1.177	1.176
trans	1.175	1.176	1.177	1.176
∡ FeNO	142.5	–	–	–
∡ FeNN	76.8	179.8	75.3	180.0
∡ NNO	140.6	179.8		
ν_{NNO}	1159, 659	2287, 1120	–	–
ν_{NN}	1812		2100	2167
ν_{CN}	2127–2147	2114–2131	2106–2116	2115–2126

[a]Distances in free N$_2$O: N–N, 1.1282 Å; N–O, 1.1842 Å.

[b]Fundamental IR wavenumbers in free N$_2$O: ν_1 (asymmetric stretch), 1285 cm^{-1}; ν_2 (bending), 589 cm^{-1}; ν_3 (symmetric stretch), 2224 cm^{-1}.

[c]N–N distance in free N$_2$, 1.10 Å; N–N distance in [Ru(NH$_3$)$_5$(η^1-N$_2$)]$^{2+}$, 1.12 Å.

[d]See text for comparisons with η^1- and η^2-complexes of [Os(NH$_3$)$_5$N$_2$]$^{2+}$. Data related to *a–d* were taken from Refs. (*78,80,81*).

linear addition mode was proposed (*75*). Interestingly, the cyclic adduct geometry was compatible with the labeling experiments, but it was rejected without further consideration. Our calculations do not render a stable species for the linear adduct of NP with azide. As to the alternative decomposition paths, Fig. 17(a,b) show two possible modes differing in the different cleavage paths of the bound cyclic adduct. On the other hand, Fig. 17(c) describes an OH$^-$ substitution-promoted azide dissociation, which further decomposes to N$_2$ and N$_2$O products. A detailed theoretical analysis considering solvent effects on the energetics of each of the different paths has been considered (*67*).

E. REACTIVITY OF NP WITH ALIPHATIC AMINES IN ORGANIC SOLVENTS

The reactions of NP with different aliphatic amines (ethyl-, *n*-propyl-, *n*-butyl-, cyclohexyl-, and benzylamines) and amino acids have
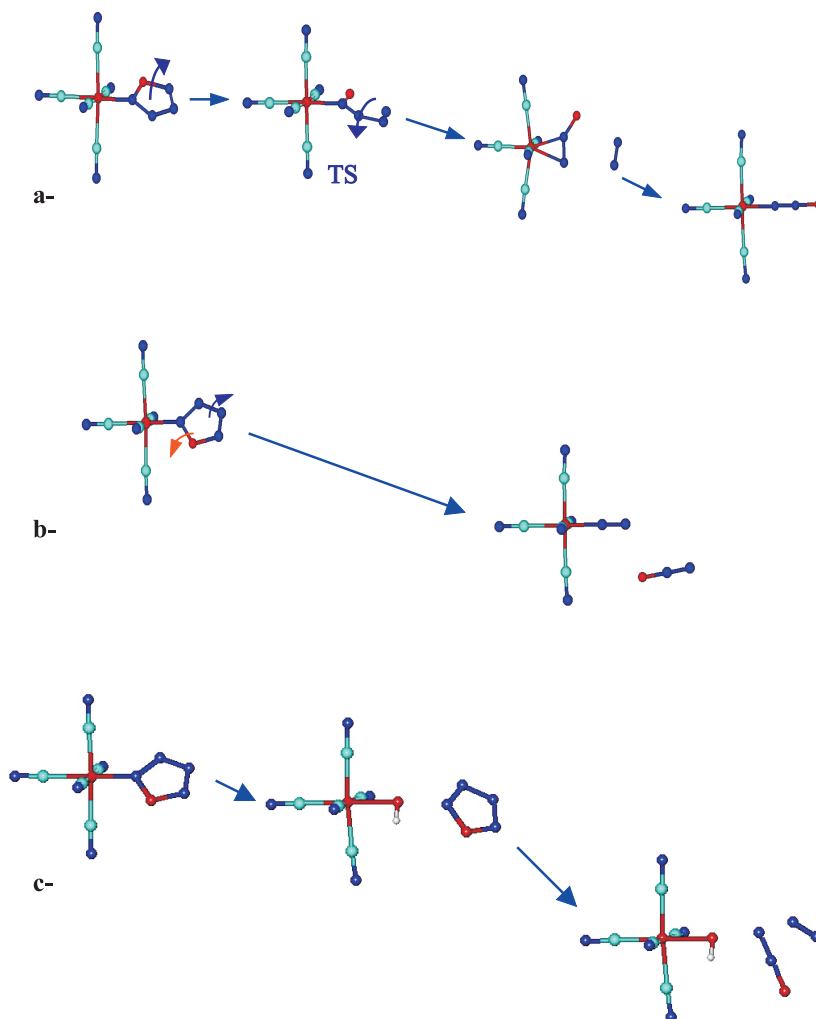
FIG. 17. Possible decomposition paths of the cyclic adduct formed by reaction of $[Fe(CN)_5NO]^{2-}$ with azide. (a) N_2 release and stabilization of the N_2O-bound intermediates. (b) N_2O release and stabilization of the N_2-bound intermediate. (c) N_4O release promoted by OH^- substitution. The cyclic species decomposes to give N_2O and N_2 in a reaction that is exothermic by 60 kcal mol^{-1}. The structures correspond to single points on the potential hypersurface, calculated at the B3LYP/6-31G** level. Relative energies are not drawn to scale. Arrows indicate changes in the molecule that lead to the next step.

been studied in aqueous solution (*83*). The stoichiometry of the reactions is:

$$[Fe(CN)_5NO]^{2-} + RNH_2 + OH^- \longrightarrow [Fe(CN)_5H_2O]^{3-} + N_2 + ROH$$

(23)
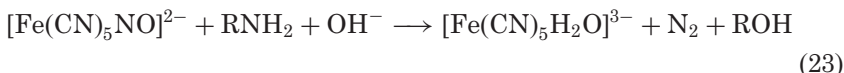
Nitrosation, diazotation, and deamination processes take place in the reactions resulting in alcohols and N_2 gas as final products. From the studies on the pH-dependence of the rate constants at different temperatures, a mechanism was proposed involving diazonium ions as intermediates. With the prediction that coordination to the metal could stabilize the otherwise extremely reactive diazonium species, the mechanism of these reactions are being studied in organic media.

The reactions of $[M(CN)_5NO]^{2-}$ (M = Fe, Ru, Os) with lithium *n*-butylamide were recently reported (*84*). Free (*E*)-*n*-butyldiazoate was found as the only product arising from the amide. The intermediate diazoate complex is labile and therefore it is rapidly replaced by other ligands present in the reaction medium. This result provides a strong indication that diazoates (and/or diazoic acids) are intermediates in the reactions of amines with these nitrosyl complexes. This is consistent with a mechanism described in Fig. 18, in which one equivalent of amide adds nucleophilically to the nitrosyl, while a second equivalent rapidly abstracts a proton from the diazoic acid before it decomposes producing a diazonium ion.

When the same reaction was carried out with (tba)$_2$[Ru(CN)$_5$NO] and (tba)$_2$[Os(CN)$_5$NO], signals attributable to *n*-butyldiazoate were observed again by ^{13}C NMR. Indirect UV–Vis evidence indicates that the diazoate complex is labile enough as to be substituted by
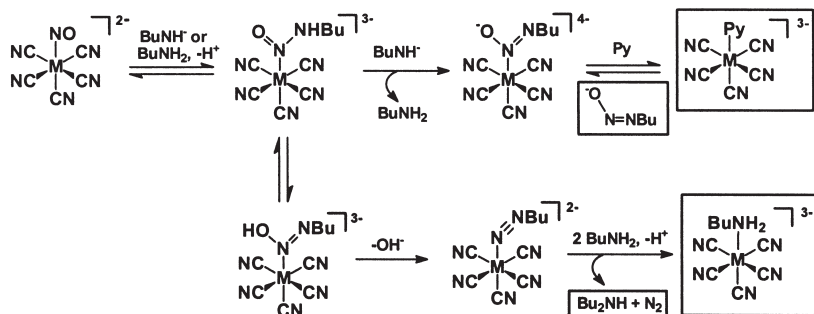

FIG. 18. Proposed mechanism for the reactions of lithium *n*-butylamide and *n*-butylamine with $[M(CN)_5NO]^{2-}$ (M = Fe, Ru, Os).

other ligands present in the reaction medium (such as pyridine used as a co-solvent) even in the case of the inert osmium complex.

The formation of n-butyldiazoate by reaction of $[Fe(CN)_5(NO)]^{2-}$ with lithium n-butylamide contrasts with the formation of dibutylamine as the main product in the reaction of the same complex with n-butylamine (*85*). This can be explained if the diazoic/diazoate equilibrium shown in Fig. 18 is shifted to the left far enough to form of a diazenido by loss of hydroxide. Attack of n-butylamine on the α-carbon of the diazenido species, produces dibutylamine. DFT computed results suggest that the stabilization by complexation of the intermediate diazonium ion (see Fig. 18) is large for the iron-pentacyano complex, in agreement with the fact that no rearrangement products were observed in the reaction of this species with n-butylamine (*86*). The reaction has been proposed as a good route for the preparation of symmetrical, unsymmetrical, and cyclic second-ary amines (*85*).

On the other hand, $[Fe(CN)_5NO]^{2-}$ reacts with benzylamine, $PhCH_2NH_2$, to produce mainly *N*-benzylphenyl-methanimine and PhCN as oxidation products (the latter one only in the presence of oxygen). $(PhCH_2)_2NH$, $PhCH_2Cl$, and $PhCH_2OH$ are produced as diazotization products. Products derived from the benzyl radical $PhCH_2^{\bullet}$ (such as PhMe), are also formed, a fact that suggests that the benzyl radical is an intermediate. Since oxidation products are generated even in the absence of oxygen, a mechanism in which the nitrosyl ligand acts as an oxidant has been proposed (*87*).

F. REACTIVITY OF NP WITH TRIOXODINITRATE, $N_2O_3^{2-}$

A kinetic study of the reaction of NP with $N_2O_3^{2-}$ (the anion of Angeli's salt (*13*)) has been performed in the pH range 5–11, at different relative concentrations of the reactants (*88a*). UV–Vis and mass-spectrometric techniques have been used, including ^{15}N labeling at the N-1 position of trioxodinitrate, $^-ON^1{=}N^2O_2^-$. A fast production of nitrite was observed and Eq. (24) was proposed:

$$[Fe(CN)_5NO]^{2-} + HN_2O_3^- \longrightarrow NO_2^- + products \qquad (24)$$

The initial product was described as $[Fe^{II}(CN)_5(NO^+NO^-)]^{2-}$ (I), formed after the nucleophilic addition of the N-1 atom of $HN_2O_3^-$ to the bound nitrosyl, with further cleavage of the N=N bond in $HN_2O_3^-$. The evolution of NO and N_2O was observed at the early stages of the

reaction, together with the formation and decay of complex I. Complex I was proposed to be the precursor of NO release, with formation of an intermediate complex II, absorbing at 410 nm, which was identified as $[Fe(CN)_5NO]^{3-}$. It was suggested that II decomposed to $[Fe^{III}(CN)_5 H_2O]^{2-}$ and NO^-, with the nitroside ion acting as the precursor of N_2O.

In spite of the detailed mechanistic study, the nature of intermediates I and II seems not to be clearly defined. The maximum at 410 nm should not be ascribed to the $[Fe(CN)_5NO]^{3-}$ ion, which, on the other hand, shows a main absorption at 345 nm and a lower intensity one at 440 nm (*40*). Furthermore, the $[Fe(CN)_5NO]^{3-}$ ion is not expected to decompose intramolecularly leading to NO^-; instead, it is known to release NO very slowly (see above). Certainly, $[Fe(CN)_5NO]^{3-}$ could be converted to other products under oxidative or reductive conditions, and this is an issue that merits further investigation. As a conclusion, the mechanistic scheme, and the crucial issue dealing with the characterization and mechanism of formation of the NO^- or HNO species as precursors to N_2O still remain uncertain.

A related kinetic and mechanistic study was performed for the same nucleophile reacting with the $[Ru(NH_3)_5NO]^{3+}$ cation (*88b*). The initial stages suggested a similar route as described before, but a significant difference was shown through the different splitting mode of $N_2O_3^{2-}$, leading this time to free NO and bound nitrite. These reactions, together with the previously studied one of trioxodinitrate with nitrous acid (*88c*), offer an interesting set for valuable comparisons on the influence of the fragments bound to NO^+ in the stoichiometry and mechanistic features of the corresponding nitrosation processes. However, to make this possible, they should be revisited.

VI. The Autooxidation of Hydrazine

The redox reactions of hydrazine toward main-group and transition metal oxidants have been reviewed (*73*). Different stoichiometries have been found, with N_2 appearing as the N-containing oxidized product, sometimes accompanied by the formation of NH_3 and/or HN_3. The mechanisms have been analyzed in terms of the one- or two-electron nature of the oxidants, and imply both outer- and inner-sphere routes, depending on the oxidant. The very reactive, key intermediate, diazene (diimide), N_2H_2, has been proposed in most of these reactions.

The reaction with O_2 is absent from these studies. It turns out that the autoxidation reaction should be a very slow process because of

kinetic barriers. It has been known for a long time that traces of aqueous metal ions (Cu, Fe) catalyze the oxidation of hydrazine to dinitrogen by dissolved oxygen (*89*). Assuming that coordination is involved, no mechanistic studies are available, however, probably because of the difficulties associated with intermediate detection in such labile systems. Pentacyanoferrates(II) are known to form stable, well characterized complexes with hydrazine (*90a*), and the ligand interchange kinetic properties have been described (*90b*). Traces of the labile pentacyano(L)ferrate(II) ions (L $=$ H$_2$O, NH$_3$, N$_2$H$_4$, etc.) are able to decompose large quantities of hydrazine upon O$_2$ exposure in a catalytic way, with release of N$_2$ (*91*). Mixtures prepared in approximately equimolar conditions of [Fe^{II}(CN)$_5$NH$_3$]$^{3-}$, O$_2$, and N$_2$H$_4$ developed orange-to-red colors, which decayed if more O$_2$ was introduced in the medium, showing N$_2$ release. Experiments performed under different conditions enabled to detect two intermediates absorbing at 440 and 515 nm. Although the first one was assigned to the [Fe^{III}(CN)$_5$N$_2$H$_4$]$^{2-}$ ion, complementary experiments performed later suggest that the 440 nm band, which is a precursor of the one at 515 nm, should be related to the mononuclear [Fe(CN)$_5$N$_2$H$_2$]$^{3-}$ ion. The second absorption at 515 nm was proposed to be associated with the diazene-bridged complex, [(NC)$_5$ Fe^{II}HN=NHFe^{II}(CN)$_5$]$^{6-}$ (*91*). Although the molar absorptivity of the 515 nm band could not be measured because of its transient character, the order of magnitude is certainly around 10^3 M^{-1} cm^{-1}, suggesting an MLCT transition from Fe(II) to the vacant diazene orbital. More conclusively, the Resonance Raman spectrum obtained with argon ion laser irradiation showed an absorption at 1440 cm^{-1}, assignable to the N=N stretching vibration. Figure 19 describes a simplified mechanism for the catalytic process.

The high lability of bound N$_2$ in [Fe^{II}(CN)$_5$N$_2$]$^{3-}$ regenerates the active site, namely the [Fe^{II}(CN)$_5$H$_2$O]$^{3-}$ ion, which is able to further bind and process hydrazine. A more detailed kinetic study could be warranted for this interesting set of reactions. Some uncertainties still remain as to the nature of the intramolecular electron-transfer rate processes (*91*). At the employed concentration levels of the complex, the participation of mixtures of mononuclear and dinuclear complexes complicate the spectral evolution. Even the nature of the dinuclear intermediates (cyano- or hydrazino-bridged) could be put into question (probably both are involved, due to the labile interconversion equilibria). The participation of Fe(III) species, either in the mononuclear or dinuclear species, as reactive intermediate precursors of the formation of diazene and N$_2$
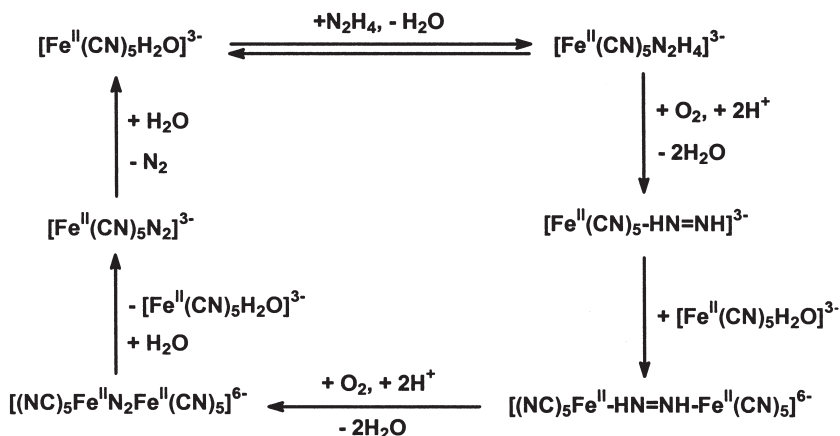
$$[Fe^{II}(CN)_5H_2O]^{3-} \xrightleftharpoons{+N_2H_4, -H_2O} [Fe^{II}(CN)_5N_2H_4]^{3-}$$

$+ H_2O$
$- N_2$

$+ O_2, + 2H^+$
$- 2H_2O$

$$[Fe^{II}(CN)_5N_2]^{3-} \qquad\qquad [Fe^{II}(CN)_5\text{-HN=NH}]^{3-}$$

$- [Fe^{II}(CN)_5H_2O]^{3-}$
$+ H_2O$

$+ [Fe^{II}(CN)_5H_2O]^{3-}$

$$[(NC)_5Fe^{II}N_2Fe^{II}(CN)_5]^{6-} \xleftarrow[- 2H_2O]{+ O_2, + 2H^+} [(NC)_5Fe^{II}\text{-HN=NH-}Fe^{II}(CN)_5]^{6-}$$

FIG. 19. Catalytic cycle promoted by the $[Fe(CN)_5H_2O]^{3-}$ ion, for the reaction of hydrazine with O_2, giving N_2, with the intermediate formation of bound diazene as mononuclear and dinuclear complexes.

complexes, is highly feasible, but has not been proved. Certainly true, however, are the gross stoichiometric features of the catalytic process, involving the oxidation of hydrazine through two successive $2e^-$ steps, and the participation of bound diazene complexes as intermediates. Recent spectroscopic evidence on related systems is available for sustaining the latter point (*92*). The successive two-electron transfers are highly feasible for O_2 and transiently formed H_2O_2 acting as oxidants in the overall reaction process, most probably through a mechanistic path involving association of the reactants (cf. the auto-xidation of $[Fe^{II}(CN)_5H_2O]^{3-}$ to $[Fe^{III}(CN)_5H_2O]^{2-}$, see below).

VII. The Oxidation of Amines and Alcohols

Oxidative dehydrogenation reactions of alcohols and amines are widespread in enzymatic biochemistry, and are of potential importance with regard to the operation of fuel cells based on simple alcohols such as methanol. The nature of products, and their rates of formation, may vary depending on the reaction conditions, and a role of metal ions has been recognized. The oxidation of amines may lead to a variety of products (nitriles, nitro species, etc.) although dehydrogenated diimine products are obtained quantitatively when the oxidation of the amine occurs via coordination to metal centers. A review is available on the mechanisms of oxidative dehydrogenations of coordinated amines and alcohols (*93*).
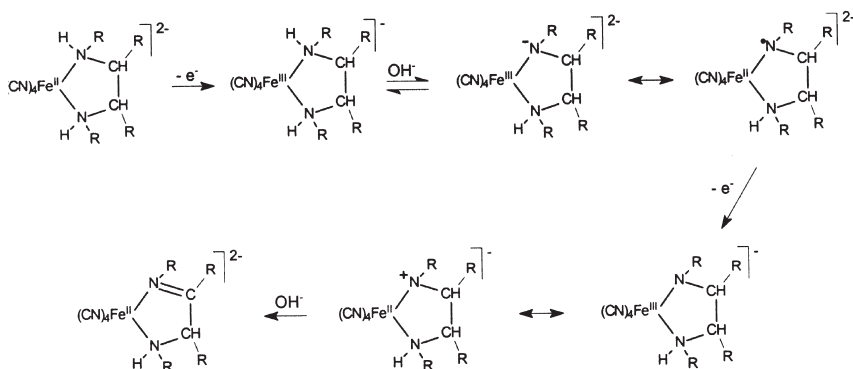
Fɪɢ. 20. Proposed mechanism for the oxidation of chelating diamine ligands bound to $[Fe^{II}(CN)_4]^{2-}$, with formation of different intermediates involving Fe^{II}, Fe^{III} species, and final formation of the $[Fe^{II}(CN)_4(diimine)]^{2-}$ complexes.

A large amount of work has been devoted to N-binding macrocyclic complexes of Ni, Cu and Fe, which yield imine ligand products. Bidentate amine ligands, mainly ethylenediamine (en), have been used with Ru and Os complexes. The oxidation of coordinated ethylenediamine and related ligands stops at the diimine stage and does not continue to the dinitrile. The α,α'-diimine entity –N=C–C=N– formed in the four-electron oxidation is particularly stable (*93*).

Ligand oxidations have been studied within a series of complexes of the type $[Fe^{III}(CN)_4(1,2\text{-diamine})]^-$ {1,2-diamine = ethylenediamine, (*R*)-1,2-diaminopropane, (*R,R*)-1,2-diaminocyclopentane, (*R,R*)-1,2-diaminocyclohexane, *N,N'*-dimethylethylenediamine} and $[Fe^{III}(CN)_4$ {2-(aminomethyl)pyridine}]$^-$. The results have been interpreted in a similar manner to the macrocyclic complexes (*94–96*). Related autoxidation processes have been published, particularly with the $[Fe^{II}(CN)_4(en)]^{2-}$ complex, leading to deep-red ethylenediimine derivatives (*97*). The Fe(II) species undergo oxidative dehydrogenation induced by a variety of oxidants, such as O_2, H_2O_2, and $[Fe(CN)_6]^{3-}$. Figure 20 shows the proposed mechanism for the dehydrogenation reactions of the above mentioned diamines. The initial Fe(II) species is oxidized to Fe(III), and a base-assisted deprotonation occurs. Deuterium isotope effect studies confirmed the site as the N–H rather than the α-CH bond. Intramolecular electron transfer from the deprotonated nitrogen atom to the Fe(III) center allows the formation of a Fe(II) radical species, which is subsequently oxidized to an Fe(III) radical analogue. A further intramolecular electron transfer from the nitrogen radical

to Fe(III) generates a putative Fe(II) cationic species. Proton release may then occur to form the imine product.

Alternatively, the effective role of the ruthenium and osmium centers in promoting the oxidative dehydrogenation of amine and alcohol ligands has been traced to their ability to attain an oxidation state two units greater than the final state, using a non-radical mechanistic route. As shown in Fig. 20 for the iron derivatives, the proposed intramolecular one-electron oxidation steps involve ligand-radical species, but the possibility of a similar mechanism for iron through the formation of Fe(IV) intermediates has been raised. The question remains ambiguous (*93*).

Given the characterization of mononuclear $[Fe(CN)_5(en)]^{3-}$ (*98*), as well as of other bound diamines (*99*), their ability toward reactive dehydrogenation could be expected, probably in a more effective way if dinuclear complex formation is allowed for. Some precedent exists for the autoxidation of bound 4-aminomethylpyridine to 4-cyanopyridine in $[Fe(CN)_5]^{3-}$ (*100*). The preparation of these putative dinuclear complexes, bridged by unsaturated diimine ligands could be an interesting issue, reinforced by the possibility of preparing new mixed-valence species, and stimulated by the renaissance experienced in this field, related to the diverse electronic delocalization patterns (*9,10*).

The reaction between $Na_2[Fe^{III}(CN)_5NH_3] \cdot H_2O$ and various aromatic amines and nitrogen heterocycles was originally investigated as a color reaction for the determination of the organic compounds (*101*). Amino compounds such as *p*-phenylenediamine generate coordinated quinone-imine complexes bound to pentacyanoferrate(II) (*102*). By extending the work to the reactions of the Fe(III) compound with *p*-aminophenol, it has been shown that the oxidized *p*-aminophenoxyl radical can be stabilized in the $[Fe^{II}(CN)_5]^{3-}$ fragment. The complex has been isolated as a zinc salt and evidence for the bound radical has been provided through IR, EPR, and Moessbauer measurements (*103*).

VIII. The Disproportionation of Hydroxylamine

Disproportionation reactions of "free" NH_2OH have earlier been reported to produce N_2, N_2O, and NH_3 (*104*). Given that these processes are very slow, it has been proposed that they should have originated from metal ion impurities, suggesting that previous coordination of NH_2OH is a prerequisite to disproportionation (*105*). Unfortunately, the redox properties of coordinated

NH_2OH as compared to the uncoordinated ligand have not been studied in great detail (*104*). Coordination of NH_2OH to the metal and further attack by another NH_2OH have been proposed for the initial step in the disproportionation of NH_2OH to N_2 and NH_3 by the labile $[Ni(CN)_4]^{2-}$ ion in anaerobic medium. The participation of $[Ni(CN)_3(NO)]^{2-}$, containing the nitroside anion, has been proposed as an intermediate precursor for the formation of products (*106*). Other evidences have been reported in the literature on the role of iron complexes catalyzing the disproportionation reactions. This is the case for NP (*75*), as well as for soluble iron–nitrosyl porphyrins reacting with NH_2OH (*107*). However, neither detailed kinetic studies nor even a rigorous stoichiometric picture have been provided.

The NH_2OH disproportionation reaction catalyzed by NP (*75*) was considered in a detailed kinetic study, performed spectrophotometrically and gas volumetrically (*108*). The found products were N_2, N_2O, and NH_3, and a mechanistic interpretation identified a fast route, probably effected by radicals derived from a bridged hydroxylamine dinuclear complex. The slow route was associated with the intermediacy of a nitroside complex.

The above results and interpretation show no conclusive evidence for the proposed paths, given the complexity of the product distribution and its dependence on different medium conditions. The reaction process is currently being revisited (*63*), using $[Fe(CN)_5NH_3]^{3-}$ in place of NP as a starting reagent and as a controlled source for the expected active catalyst, $[Fe(CN)_5H_2O]^{3-}$. Ongoing investigations confirm the nature of the above reaction products, establishing the required conditions for obtaining mixtures of N_2/N_2O in different proportions, as well as exclusively N_2. Most remarkably, the studies demonstrate that NP is also an important oxidation product of NH_2OH in particular conditions. It can be shown that small amounts of $[Fe(CN)_5NH_3]^{3-}$ are able to process much larger amounts of NH_2OH, with reproducible cycling. The participation of mononuclear and cyano-bridged dinuclear intermediates can be described, as well as of Fe(II)–Fe(III) intermediates. The mechanistic proposal has an impressive resemblance with the reduction and oxidation reactions of NH_2OH carried out by the relevant enzymes acting in the natural systems, which effect, on the one hand, the reduction of NH_2OH to NH_3 (*109*), and, on the other hand, the oxidation to nitrite (*69*). The latter process apparently involves successive two-electron oxidation steps leading to Fe^{II}–HNO and Fe^{II}–NO$^+$ intermediates, with final conversion to nitrite and release to the medium.

IX. Miscellaneous Reactions

A. The Reaction of $[Fe(CN)_5H_2O]^{3-}$ with O_2 and H_2O_2

The stoichiometry of the autoxidation reaction was earlier established (*7a,7c*) as:

$$4[Fe^{II}(CN)_5H_2O]^{3-} + 4H^+ + O_2 \longrightarrow 4[Fe^{III}(CN)_5H_2O]^{2-} + 2H_2O \quad (25)$$
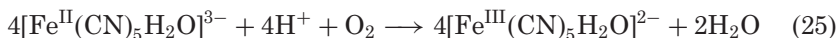
Reaction (25) is remarkable, because the aqua complex ion has a very similar redox potential as the hexacyano-complex (ca. 0.40 V), and the latter is known to be unreactive toward oxygen (*1*). The mechanism of reaction (25), comprising the one-electron reduction of O_2 to O_2^- as an initial step through an outer-sphere route, appears to be endergonic, and therefore other mechanistic paths should be considered. Toma demonstrated elegantly in 1975 (*6a*) that the rate of reaction (25) was very slow, and was influenced by the presence of spurious ferrous ions, which are always present in aged solutions of $[Fe(CN)_5H_2O]^{3-}$. By performing systematic studies with added ferrous ions, as well as using chelating species as inhibitors, he provided strong evidence that a catalytic mechanism was underway, based on the rate law: $-d[Fe(CN)_5H_2O^{3-}] = k_3$ $[Fe(CN)_5H_2O^{3-}]$ $[O_2]$ $[Fe_{aq}^{2+}]$, with $k_3 = 5.6 \times 10^6$ M^{-2} s^{-1}, at $25\,^\circ C$, $I = 0.1$ M, pH 4.5. Kinetically indistinguishable structures for the activated complexes were proposed, involving either end-on or bridged O_2 structures between the associated pentacyano and Fe_{aq}^{2+} species. A similar picture appears for the oxidation of pentacyano and hexacyano complexes with hydrogen peroxide (*110*). Reaction (25) was studied in very diluted complex solutions, ca. 10^{-5} M, where the mononuclear aqua ion is highly predominant. Our own preliminary results show that the oxidation also develops in more concentrated solutions, with a significant presence of the cyano-bridged mixed-valence dinuclear complex, as revealed by the appearance of NIR absorptions, in addition to the absorptions in the near UV region (*111*).

B. The Coordination Chemistry of Sulfite

The electrophilic reaction of NP with sulfite (the Boedeker reaction) has been studied, and follows a similar reaction pattern as with other reactants [Eqs. (5) and (6)]. The red color shows up at 475 nm, and this decays in an unknown way with formation of $[Fe(CN)_5SO_3]^{5-}$ as the

final product. A strong influence of the type of alkaline countercations has been observed on the spectroscopic and reactivity properties, consistent with the highly negative charges afforded by the reactants (*28*). A related adduct has been prepared by the reaction of sulfite with *cis*-[RuCl(bpy)$_2$NO]$^{2+}$ allowing for the determination of the crystal structure of the adduct, *cis*-[RuCl(bpy)$_2$\{N(O)SO$_3$\}]. This is the first adduct for which structural data exists, demonstrating the addition of the nucleophile to the N atom of nitrosyl (*28*).

The [Fe(CN)$_5$SO$_3$]$^{5-}$ ion has been prepared and characterized as a sodium salt (*112*). By reacting with one equivalent of the oxidizing agents [Ir^{IV}Cl$_6$]$^{2-}$and [Fe^{III}(CN)$_6$]$^{3-}$, it can be oxidized to the Fe(III) analogue (*113*), as also observed with excess S$_2$O$_8^{2-}$ (*114*). An exploration of the reactions of the Fe(III) complex with excess oxidant leads to free sulfate, with the intermediacy of ill-characterized colored intermediates (*113*).

The reactivity of [Fe(CN)$_5$SO$_3$]$^{5-}$ toward reduction has not been investigated. However, a report on the closely related [Ru^{II}(NH$_3$)$_5$(SO$_2$)]$^{2+}$ ion described its electrochemical reduction to [Ru^{II}(NH$_3$)$_5$(H$_2$S)]$^{2+}$ (*115*), where the sulfur ligand remains bound through the net six-electron change. The [Fe^{III}(TPPS)(H$_2$O)$_n$]$^{3-}$ complex ($n=1$ or 2), which was shown above to mimic the action of a NiR enzyme in its ability to reduce NO$_2^-$ to NH$_3$ catalytically (*64*), is also an effective electrocatalyst for the reduction of HSO$_3^-$ to H$_2$S (*116*), a process that occurs in nature via a stepwise process that is carried out by the sulfite reductase enzymes (*117*). Given the commented analogies between the pentaammineruthenium and pentacyanoferrate chemistry (*79*), as well as the previously described catalytic nitrite reduction processes associated with the pentacyanoferrates(II), it seems that the issue of sulfite reduction in the latter system could be an attractive challenge.

C. THE REACTION OF [Fe(CN)$_5$L]$^{n-}$ (L = NO$^+$ AND H$_2$O) WITH SH$^-$ AND THIOLATES, SR$^-$

The electrophilic reactions of NP with SH$^-$ and several SR$^-$ have been studied and reviewed (*28*). The nature of the reversible addition reactions [Eq. (5)] are reasonably well understood for the thiolates. A kinetic study including some bioinorganically relevant nucleophiles (cysteine, glutathione) was performed by using stopped-flow and T-jump techniques (*77*). The rate constants for the forward and reverse processes in Eq. (5) were in the range 10^3–10^4 M^{-1} s^{-1} and 10^1–10^3 s^{-1} at 25 °C, respectively.

The typical red colors (absorptions at ca. 522–526 nm, with $\varepsilon = 10^3$–10^4 M^{-1} cm^{-1} (*118*), for different structurally related thiols and thiolates) strongly suggest that the binding of the nucleophile occurs through the sulfur atom and the N atom of nitrosyl, and are most probably associated with MLCT transitions. The intensities of these absorptions are larger in alkaline media, suggesting that previous deprotonation of sulfur is occurring. Although no crystal structures of the adduct species are available, a recent IR study of the reaction of NP with EtSH (*119*) demonstrated that the {Fe^{II}–NO(SEt)} moiety is present, on the basis of ν_{NO} found at 1380 cm^{-1}, which is consistent with a double N=O bond and also with a similar electronic distribution to the one previously discussed for the addition of OH^- and N-binding nucleophiles to NP.

The addition reactions of thiolates to NP are generally followed by the decomposition of the red adducts. A survey on the persistence of the red colors showed that the adduct with thiosuccinic acid was extremely stable over days (*118*). Some rationalization on the different adduct stabilities has been advanced; thus, the presence of electron-rich or electron-withdrawing groups on the thiolate anion destabilize or stabilize the adducts, respectively. The great stability of the thiosuccinic acid adduct with NP has shown to be valuable for the quantitative determination of the nitrosyl complex (*34,35*).

The decomposition mode of the adducts has early been noticed to be associated with redox reactions (*60,77*), and is currently under scrutiny because of its great bioinorganic relevance. It has been shown that the reduction of NP to the EPR-active $[Fe(CN)_5NO]^{3-}$ ion occurs in the reaction with cysteine, which is oxidized to cystine (*60*). In this reaction, NP showed to behave catalytically with respect to the autoxidation of cysteine to cystine, provided enough oxygen was present. A recent kinetic and mechanistic study has thrown more light on the complex mechanistic details comprising the decompositions of the red adducts formed by NP with cysteine, *N*-acetylcysteine, ethyl cysteinate, and glutathione (*120*). Under conditions of excess of NP, in anaerobic medium, the reversible adduct formation step is shown by Eq. (26):

$$[Fe(CN)_5NO]^{2-} + RS^{n-} \rightleftharpoons [Fe(CN)_5N(O)SR]^{(n+2)-} \qquad (26)$$

Reaction (26) is followed by a first order process, which has been interpreted as an homolytic splitting of the N–S bond, Eq. (27), with formation of the one-electron reduction product of NP, $[Fe(CN)_5NO]^{3-}$,

and thiyl radicals that are the precursors of disulfide formation, RSSR. In the related reaction of NP with SEt^-, the decay of the IR absorption at 1380 cm^{-1}, corresponding to the red $[Fe(CN)_5N(O)SEt]^{3-}$ adduct (*119*), correlates with the increase at 1648 cm^{-1} for $[Fe(CN)_5NO]^{3-}$, as predicted by Eq. (27):

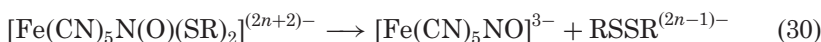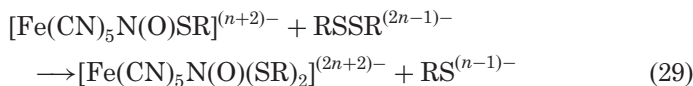$$[Fe(CN)_5N(O)SR]^{(n+2)-} \longrightarrow [Fe(CN)_5NO]^{3-} + RS^{(n-1)-} \qquad (27)$$

The rates depend on the thiol structure, and correlate well with inductive effects. Thus, the $-NH_2$ and COO^- groups destabilize and stabilize the red adduct, respectively. When the groups are blocked by acetylation or esterification, their influence is suppressed, as shown by *N*-acetylcysteine, which forms the most stable adduct in the series because of the unprotected COO^- and the acetylated amino group.

Figure 21 shows a reaction scheme for the above reactions. The scheme also includes the distinct behavior under excess thiolate conditions, which reveals a faster adduct decomposition. The kinetics are complicated, showing induction periods that are indicative of autocatalysis through a chain reaction initiated by the $RS^{(n-1)-}$ radicals, Eq. (28):

$$RS^{(n-1)-} + RS^{n-} \rightleftarrows RSSR^{(2n-1)-} \qquad (28)$$

These radicals can be scavenged by both complexes in Eq. (26). Chain propagation is proposed to occur through Eq. (29), forming a dithiolato transient species that reacts according to Eq. (30).

$$[Fe(CN)_5N(O)SR]^{(n+2)-} + RSSR^{(2n-1)-}$$
$$\longrightarrow [Fe(CN)_5N(O)(SR)_2]^{(2n+2)-} + RS^{(n-1)-} \qquad (29)$$

$$[Fe(CN)_5N(O)(SR)_2]^{(2n+2)-} \longrightarrow [Fe(CN)_5NO]^{3-} + RSSR^{(2n-1)-} \qquad (30)$$

Reactions (28–30) generate additional quantities of the $RSSR^{(2n-1)-}$ radicals, leading to the catalysed redox decomposition of the $[Fe(CN)_5N(O)SR]^{(n+2)-}$ complex. Finally, the reaction between NP and $RSSR^{(2n-1)-}$ terminates the chain mechanism, Eq. (31).

$$[Fe(CN)_5NO]^{2-} + RSSR^{(2n-1)-} \longrightarrow [Fe(CN)_5NO]^{3-} + RSSR \qquad (31)$$

$$[Fe^{II}(CN)_5NO]^{2-} + RS^{n-}$$

$$[Fe^I(CN)_5NO]^{3-} \qquad [Fe^{II}(CN)_5N(O)SR]^{(n+2)-} \qquad \frac{1}{2}\,RSSR \qquad RSOO^{\bullet(n-1)-}$$

$$RS^{\bullet(n-1)-} \quad O_2$$

$$RS^{n-} + RS^{\bullet(n-1)-} \longleftrightarrow RSSR^{\bullet(2n-1)-} \qquad [Fe^{II}(CN)_5N(O)(SR)_2]^{(2n+2)-}$$

$$RSOO^{\bullet(n-1)-} \quad O_2 \qquad [Fe^{II}(CN)_5NO]^{2-}$$

$$\frac{1}{2}\,RSSR \qquad \qquad [Fe^{II}(CN)_5N(O)SR]^{(n+2)-} + RS^{n-}$$
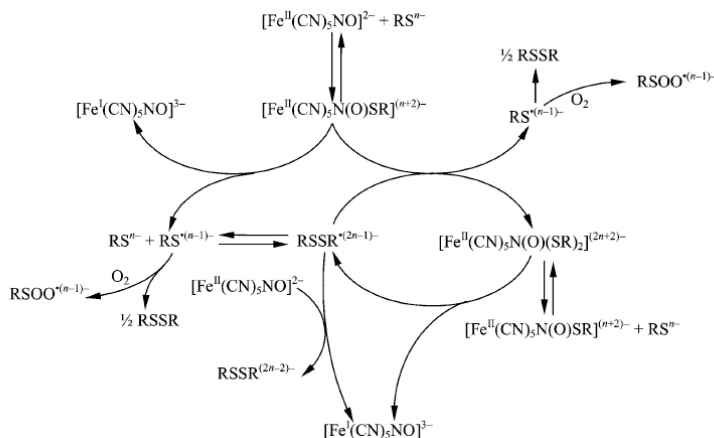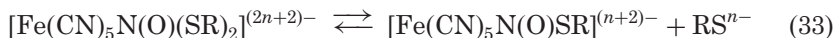
$$RSSR^{(2n-2)-}$$

$$[Fe^I(CN)_5NO]^{3-}$$
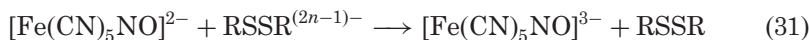
FIG. 21. Proposed scheme for the reactions of NP with thiolates, RS^{n-}, showing the formation and spontaneous homolytic splitting of the adduct, $[Fe(CN)_5N(O)SR]^{(n+2)-}$, followed by autocatalytic redox reactions proceeding with thiolate excess, in anaerobic medium. The influence of oxygen is also included for some of the reactions.

Reactions (32–33) may also contribute to the termination of the catalytic cycle.

$$RS^{(n-1)-} + RS^{(n-1)-} \rightleftarrows RSSR \tag{32}$$

$$[Fe(CN)_5N(O)(SR)_2]^{(2n+2)-} \rightleftarrows [Fe(CN)_5N(O)SR]^{(n+2)-} + RS^{n-} \tag{33}$$

The proposed radical mechanism presented in Eqs. (27)–(33) and Fig. 21 was also modeled with the aid of DFT calculations.

In the proposed description, the one-electron reduced product of NP, $[Fe(CN)_5NO]^{3-}$, is described as a Fe(I) species, which formally implies a NO^+ ligand. As shown above (Section III), even considering the delocalized nature of the FeNO moiety (23), there is enough spectroscopic evidence, particularly IR (36a,119), EPR (36b,37), as well as kinetic evidence (34), to support that $[Fe(CN)_5NO]^{3-}$ is best described as containing a $\{Fe^{II}NO^{\bullet}\}$ unit, with a low-spin d^6 iron species bound to a NO radical.

The overall mechanistic study shows a significant contribution to the bioinorganically relevant reactions of NP with thiolates. Although the route shown in Eqs. (26)–(33) is operative under anaerobic conditions, the study also comprised some experiments to disclose the

influence of oxygen on some of these reactions, as shown in Fig. 21, which are not discussed in detail here. As concluded by the authors, the studied systems are eventually more complex for a detailed mechanistic interpretation, because other additional equilibria comprising thiol protonations, ion pair effects and the type and concentration of countercations could be important. Moreover, the studies were performed at pH 10, where no perturbations associated with cyanide release from $[Fe(CN)_5NO]^{3-}$ are expected (see above). However, at physiological pH the latter process, involving the formation of $[Fe(CN)_4NO]^{2-}$ intermediates, has been shown to be significant. The latter species is presumably the precursor of NO release to the medium following the reduction of NP after injection ([48]). Further mechanistic studies on this process would be desirable.

An earlier report on the reaction of NP with SH^- suggests that a similar route as previously indicated for the thiolates is operative ([121]). However, the ill-defined nature of the intermediates and products has prompted a reinvestigation of this reaction. Ongoing results ([111]) show that $[Fe(CN)_5NO]^{3-}$ and sulfur are produced as primary products of the decomposition of the initially formed, red adduct. pH and other reaction conditions are shown to influence the course of the overall reaction in a still unraveled way.

The coordination chemistry of several SR^- (although not SH^-) to $[Fe^{II}(CN)_5H_2O]^{3-}$ has been studied ([122]). The complexes are not very stable (K_{st} ca. 10^3 M^{-1}) compared to other $[Fe^{II}(CN)_5L]^{3-}$ because of the high dissociation rates of the SR^- ligands (ca. 10^{-1}–10^{-2} s^{-1}). Thiolate coordination to $[Fe^{III}(CN)_5H_2O]^{2-}$ leads to fast reduction to Fe(II), with a transient appearance of blue colors, probably associated with LMCT transitions in the unstable $[Fe^{III}(CN)_5(SR)]^{3-}$ species ([111]). An independent kinetic study of the coordination and redox reactions of thiolates on Fe-aqua catalytic sites seems to be as important as the need to study the reactions with nitrosyl, given the presence of oxygen in the physiological media.

D. MODIFICATION OF ELECTRON TRANSFER REACTIVITY UPON CYANO-BRIDGE FORMATION

As anticipated above, the reactivity of the cyano complexes of transition metals are strongly influenced by the structure of the medium, namely the nature of the solvent (specific cyano-donor interactions), or the type and concentration of the counterions ([15]). Both of these factors have a profound influence in the electronic structure, and determine the observed changes in reactivity, particularly in

the electron transfer reactions, where a catalytic role of alkaline cations has been proposed (*5,16*).

When the above factors are put under control, the possibility of changing the ligand L in the pentacyano(L)ferrate complexes adds a further dimension for studying systematic reactivity changes, brought out by the controlled modification of the redox potentials of the Fe(II)–Fe(III) redox couples. In this way, the rates of electron transfer reactions between a series of $[Fe^{II}(CN)_5L]^{n-}$ complexes toward a common oxidant like $[Co^{III}(NH_3)_5(dmso)]^{3+}$ showed a variation in agreement with Marcus predictions for outer-sphere electron transfer processes, as demonstrated by linear plots of the rate constants versus the redox potentials (*123*).

Another crucial factor influencing the redox reactivity of cyano complexes is the possibility of bridging one (or more) cyano ligands to an acceptor moiety. As anticipated before, we are not attempting to discuss here the broad subject of mixed-valence chemistry, related to the intermetallic electronic coupling between metal centers, favored by the conjugated nature of cyanide or other bridging ligands like pyrazine. However, we believe that the current studies showing the ability of cyano complexes to bind on nanocrystalline and colloidal TiO_2 surfaces merits a specific comment, because of the general importance of affording a molecular approach for the conversion of light into electricity. Sensitization of these n-type semiconductors to visible light with metal cyano coordination compounds has been early recognized (*124*). Coordination of $[Fe(CN)_6]^{4-}$ to the TiO_2 surface results in the appearance of a broad absorption band around 420 nm, assigned to an Fe(II) → TiO_2 metal-to-particle charge-transfer (MPCT) band (*125a*). Surface-enhanced Raman scattering techniques have been used to estimate the vibrational reorganization energy for the MPCT intervalence transition, thus enabling the identification of the relevant internal modes associated with the interfacial charge transfer. Together with the main stretching of the cyano bridge, a number of other vibrations were found to contribute to the activation barrier, including some surface modes associated with Ti–O and Ti–N stretching (*125b*). Most important was the finding of a fast, inverted, interfacial electron-transfer behavior associated with the reverse reaction in Eq. (34).

$$[Fe^{II}(CN)_5L^{n-}]\text{--}TiO_2 \; \rightleftarrows \; [Fe^{III}(CN)_5L^{(n-1)-}]\text{--}TiO_2 \, (e) \qquad (34)$$
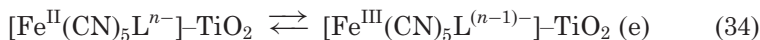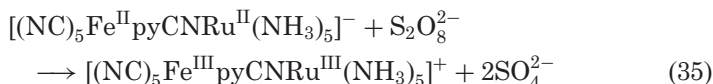
By photochemically pumping the tail of the MPCT transition, the recovery kinetics was measured in the nanosecond time scale (*125c*).

The measurements were performed with a series of $Fe^{II}(CN)_5L$ complexes (L = cyanide, py, and py-substituted derivatives) affording different redox potentials. The plot of log k_{et}, the interfacial electron transfer rate constant, versus the reduction potentials showed a negative slope, with a decreasing trend of k_{et} as the relative driving force increases, in agreement with the behavior expected for a process operating in the inverted region. Electroabsorption (Stark) spectroscopy has been used to better understand the nature of the acceptor state involved in the MPCT transition (*125d*). The average charge transfer distance determined from the Stark spectra is 5.3 Å, which is similar to the estimated distance between the Fe(II) center of the complex and the Ti^{IV} surface site, as described by $(NC)_5Fe^{II}–CN–Ti^{IV}$ (particle). It has been suggested that the electron injection is to either an individual titanium surface site or to a small number of Ti centers localized around the site of hexacyanoferrate coordination to the particle and not into a conduction band orbital delocalized over the nanoparticle.
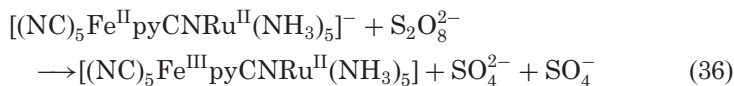
E. Intramolecular Redox Assistance of Bimolecular Redox Reactions

In spite of the abundant work on synthetic, thermodynamic, structural, and spectroscopic aspects of mixed-valence compounds, the dynamic solution behavior toward external redox reagents has not been much addressed. When such compounds are unsymmetrical and valence-localized, several problems arise when a fully reduced dinuclear complex reacts with an oxidant. Haim pioneered a systematic study performed with different systems reacting with a common two-electron oxidant, peroxydisulfate (*126*). A relevant example is given by reaction (35):

$$[(NC)_5Fe^{II}pyCNRu^{II}(NH_3)_5]^- + S_2O_8^{2-}$$
$$\longrightarrow [(NC)_5Fe^{III}pyCNRu^{III}(NH_3)_5]^+ + 2SO_4^{2-} \qquad (35)$$

In most of the reactions studied, the appearance of biphasic kinetics showed that the full oxidation process is achieved through the stepwise oxidation of one of the metal centers, rendering a mixed-valence species which is further oxidized to the final product. The question arises in Eq. (35) as to the alternative first oxidation of iron or ruthenium. The stoichiometry of the first oxidation step with bridging 4- and 3-cyanopyridines (with the N-atom of py binding to

iron and the N-atom of the nitrile group binding to ruthenium) was found to be (*127*):

$$[(NC)_5Fe^{II}pyCNRu^{II}(NH_3)_5]^- + S_2O_8^{2-}$$
$$\longrightarrow [(NC)_5Fe^{III}pyCNRu^{II}(NH_3)_5] + SO_4^{2-} + SO_4^- \qquad (36)$$

That the above redox isomer is formed instead of the $\{Fe^{II}Ru^{III}\}$ one, can be demonstrated by careful analysis of the MLCT band of the product, as well as by the properties of the intervalence (IV) band. However, it is well known that the $[Ru^{II}(NH_3)_5L]^{n+}$ ions are generally much more reactive that the $[Fe^{II}(CN)_5L]^{n-}$ analogues toward oxidation by peroxydisulfate (*126,128*), as required by the lower redox potential at the ruthenium center. A careful mechanistic analysis showed that, although the $\{Fe^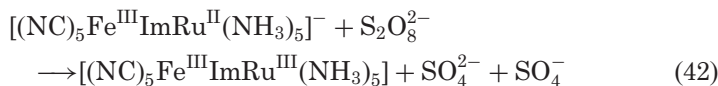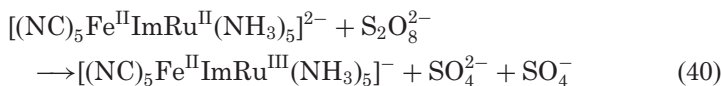{III}Ru^{II}\}$ isomer is the thermodynamically stable product, it is not the kinetically accessible one. Then, the reaction evolves as follows:

$$[(NC)_5Fe^{II}pyCNRu^{II}(NH_3)_5]^- + S_2O_8^{2-}$$
$$\longrightarrow [(NC)_5Fe^{II}pyCNRu^{III}(NH_3)_5] + SO_4^{2-} + SO_4^- \qquad (37)$$

$$[(NC)_5Fe^{II}pyCNRu^{III}(NH_3)_5] \rightleftarrows [(NC)_5Fe^{III}pyCNRu^{II}(NH_3)_5] \qquad (38)$$

$$[(NC)_5Fe^{III}pyCNRu^{II}(NH_3)_5] + S_2O_8^{2-}$$
$$\longrightarrow [(NC)_5Fe^{III}pyCNRu^{III}(NH_3)_5]^+ + SO_4^{2-} + SO_4^- \qquad (39)$$
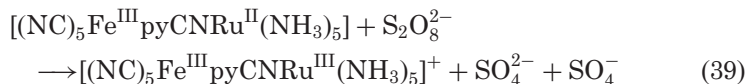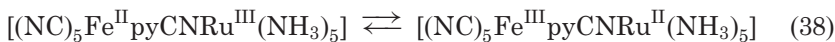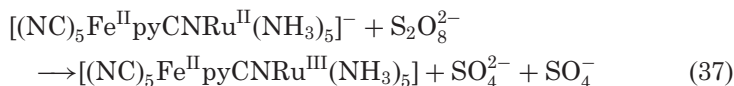
The mechanism can be described by using a $R \rightarrow M' = M \rightarrow Ox$ scheme. The fully reduced complex R is oxidized by a one-electron process to the thermodynamically unstable electronic isomer, M', which is formed by attack on the Ru^{II} center, in a kinetically controlled reaction. Then, M' rapidly isomerizes via intramolecular electron transfer to M, the thermodynamically stable isomer. As the latter species has again a very reactive Ru^{II} site, the complete oxidation to Ox is consumed. A similar mechanism has been described for the related oxidations of the $[(edta)Ru^{II}pzRu^{II}(NH_3)_5]$ complex (*129*).

A variation to the above situation is found with other complexes. By consideration of spectral results, electrochemical measurements and kinetic analysis, it has been shown that the alternative scheme $R \rightarrow M = M' \rightarrow Ox$ is operative. We illustrate this behavior for $R = [(NC)_5Fe^{II}ImRu^{II}(NH_3)_5]^{2-}$, with $Im^- =$ imidazolate ion (*130*).

$$[(NC)_5Fe^{II}ImRu^{II}(NH_3)_5]^{2-} + S_2O_8^{2-}$$
$$\longrightarrow [(NC)_5Fe^{II}ImRu^{III}(NH_3)_5]^- + SO_4^{2-} + SO_4^- \qquad (40)$$

$$[(NC)_5Fe^{II}ImRu^{III}(NH_3)_5]^- \;\rightleftarrows\; [(NC)_5Fe^{III}ImRu^{II}(NH_3)_5]^- \qquad (41)$$

$$[(NC)_5Fe^{III}ImRu^{II}(NH_3)_5]^- + S_2O_8^{2-}$$
$$\longrightarrow [(NC)_5Fe^{III}ImRu^{III}(NH_3)_5] + SO_4^{2-} + SO_4^- \qquad (42)$$

In this alternative route, the first one-electron oxidized product in Eq. (40) is the kinetically favored as well as the thermodynamically stable electronic isomer, M. The evolution of the oxidation process, is now facilitated by the rapid isomerization to the unstable electronic isomer M′ in Eq. (41), which has again an available Ru^{II} site for the reaction proceeding to Ox as in Eq. (42). This route has been also found for $R = [(NC)_5Fe^{II}bpaRu^{II}(NH_3)_5]^-$, containing the non-communicating ligand bpa $= \mu$-1,2-bis(4-pyridyl)ethane (131), and for $[(NC)_5Fe^{II}pzRu^{II}(NH_3)_5]^-$ (132).

By putting together the rate constants measured (or estimated according to the proposed models) for the relevant electron transfer steps in a broad variety of systems, including the rates found for the mononuclear $[Ru^{II}(NH_3)_5L]^{n+}$ ions, a LFER relationship was found by plotting $\ln k_{et}$ vs. E_{Ru} for the "intramolecular" electron transfer in the ion pairs $[X_5M–L–Ru^{II}(NH_3)_5]^{n+}//S_2O_8^{2-}$. The slope shown in Fig. 22 agrees with the theoretical value predicted by Marcus theory, assuming that the reorganization energies for the pentaammine–Ru(II) and –Ru(III) exchanges are insensitive to the identity of X_5ML (133).

A conclusion from these studies is that the slowly reacting X_5M fragments, such as $(NC)_5Fe^{II}$ and $(edta)Ru^{II}$, can be oxidized much faster when a rapidly reacting moiety is attached, such as $(NH_3)_5Ru^{II}$.

The discussed mechanisms represent a form of intramolecular "catalysis" of the oxidation of the $Fe^{II}(CN)_5$ or $Ru^{II}(edta)$ centers by the $Ru^{II}(NH_3)_5$ moiety. The first two moieties react sluggisly and, on the other hand, the electron in $Ru^{II}(NH_3)_5$ is readily accessible to the external oxidant and is given up. The rapid electronic isomerization processes aid in the consumption of the full oxidation process. This is not truly catalytic because the "catalyst" is the reactant itself, which, of course, is consumed in the reaction. A better description involves a net oxidation of the $Fe^{II}(CN)_5$ or $Ru^{II}(edta)$ sites through activation by the facile intramolecular electron transfer between the metal centers. The mechanism is described in Fig. 23, bearing some resemblance to the classical chemical mechanism for inner sphere electron
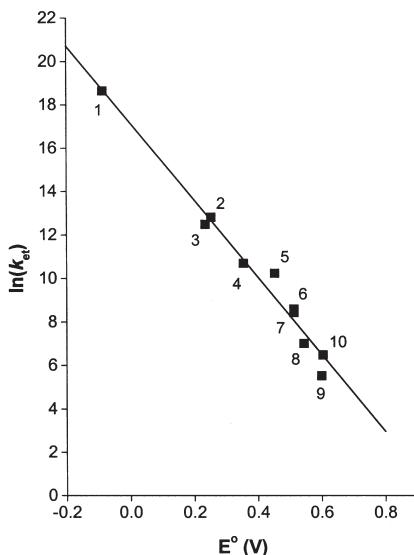
FIG. 22. Plot of $\ln(k_{et})$ vs. E°_{Ru} for "intramolecular" electron transfer in the ion pairs $[X_5M–L–Ru^{II}(NH_3)_5]^{n+}//S_2O_8^{2-}$. The $X_5M–L$ moieties are: (1) $(NC)_5Fe^{III}–Im^{3-}$; (2) $(NC)_5Fe^{II}–bpa^{3-}$; (3) $(NC)_5Fe^{III}–bpa^{2-}$; (4) $(edta)Ru^{II}–pz^{2-}$; (5) $(NC)_5Fe^{II}–pz^{3-}$; (6) $(NC)_5Fe^{II}–3pyCN^{3-}$; (7) $(NC)_5Fe^{II}–4pyCN^{3-}$; (8) $(NC)_5Fe^{III}–3pyCN^{2-}$; (9) $(NC)_5Co^{III}–pz^{2-}$; (10) $(NC)_5Fe^{III}–4pyCN^{2-}$.
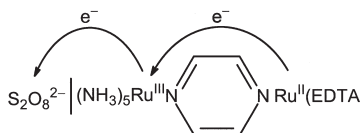
FIG. 23. Oxidation of a $Ru^{II}(edta)$ site by $S_2O_8^{2-}$, assisted by intramolecular electron-transfer mediated by the $Ru(NH_3)_5$ moiety. A similar mechanism operated for $Fe^{II}(CN)_5^{3-}$ as donor.

transfer (*126*). It is interesting to point out that the bridging ligand should not necessarily be electronic communication (cf. the bpa case), but should only favor the fast electron transfer in an appropriate geometric environment (Fig. 23).

X. Conclusions

The chemistry of redox-active ligands L in the pentacyano(L) ferrate(II) and -(III) complexes is of fundamental concern for disclosing

the mechanistic features which are operative in stoichiometric and catalytic processes associated with oxidation, reduction, and disproportionation of L. The possibility of good spectroscopic and kinetic characterization of reactants, intermediates, and products is particularly important, because these results can be obtained on a time-scale of minutes, in contrast with the difficulties found for the identification of related species associated with the much more reactive hexaaqua ions. For the Fe(II)-cyano complexes, the back-bonding ability of the metal center aids in the stabilization and eventual spectroscopic characterization of otherwise elusive intermediates, while still maintaining a sufficient lability of L in order to provide for the regeneration of Fe(II)-aqua ion as a catalytic site. This is particularly important for small molecules displaying a versatile coordination behavior, such as the *N*-binding species associated with the nitrogen redox cycle, which display complex, multi-electronic paths for oxidation or reduction in most cases, generally under kinetic rather than thermodynamic control. In addition, the relevance of the cyanometallate systems for studying the coordination and reactivity of biologically relevant S- and O-binding species has been emphasized.

The accessibility of $Fe^{II/III}$ redox states sets the basis for redox cycling, providing a possible mechanism for ligand oxidation or reduction mediated by intramolecular electron transfer between the metal and the ligand. A crucial favorable feature for the catalytic requirements is the moderate lability of water in the easily generated $[Fe^{II}(CN)_5H_2O]^{3-}$ ion, and the robust nature of the pentacyano moiety in the overall processes, with interesting exceptions such as the $[Fe^{II}(CN)_5NO]^{3-}$ ion. The lability of some L ligands may preclude however their adequate characterization in the iron systems, as shown for some intermediates such as HNO. In that case, the possibility of studying the same reactions in the more inert ruthenium and particularly in the osmium analogues should be considered, and this is also a great advantage of the systems under consideration.

By using modern DFT methodologies, the prediction and identification of reactants and intermediates in the potential energy surfaces associated with the addition reactions of different nucleophiles with nitrosyl complexes has shown to be most revealing. Although some of these intermediates (viz. the linkage isomers of N_2O) have not been detected experimentally because of the lability at the iron centers, their existence is feasible on the basis of related results obtained for other linkage isomers (NO, N_2) in low-temperature photoinduced reactions, as well as considering the reasonable results obtained for the optimized geometries and spectroscopic calculations.

REFERENCES

1. Sharpe, A. G. "*The Chemistry of Cyano Complexes of the Transition Metals*"; Academic Press: New York, 1976.
2. Dunbar, K. R.; Heintz, R. A. *Prog. Inorg. Chem.* **1997**, *45*, 283–391.
3. Macartney, D. H. *Rev. Inorg. Chem.* **1988**, *9*, 101–151.
4. Stochel, G. *Coord. Chem. Rev.* **1992**, *114*, 269–295.
5. Baraldo, L. M.; Forlano, P.; Parise, A. R.; Slep, L. D.; Olabe, J. A. *Coord. Chem. Rev.* **2001**, *219–221*, 881–921.
6. (a) Balzani, V.; Carassiti, V. "*Photochemistry of Coordination Compounds*"; Academic Press, 1970, Chap. 5; (b) Stasicka, Z.; Wasielewska, E. *Coord. Chem. Rev.* **1997**, *159*, 271–294; (c) Szacilowski, K.; Macyk, W.; Stochel, G.; Stasicka, Z.; Sostero, S.; Traverso, O. *Coord. Chem. Rev.* **2000**, *208*, 277–297.
7. (a) Toma, H. E. *Inorg. Chim. Acta* **1975**, *15*, 205–211; (b) Toma, H. E.; Malin, J. M. *Inorg. Chem.* **1974**, *12*, 1772–1774; (c) Kenney, D. J.; Flynn, T. P.; Gallini, J. B. *J. Inorg. Nucl. Chem.* **1961**, *20*, 75; (d) Brauer, G. "*Handbook of Preparative Inorganic Chemistry*", Vol. 2, 2nd edn.; Academic Press: New York, NY, 1965, p. 1511.
8. Zerga, H. O.; Olabe, J. A. *Inorg. Chem.* **1983**, *22*, 4156–4158.
9. Kaim, W.; Klein, A.; Gloeckle, M. *Acc. Chem. Res.* **2000**, *33*, 755–763.
10. (a) Demadis, K. D.; Hartshorn, C. M.; Meyer, T. J. *Chem. Rev.* **2001**, *101*, 2655; (b) Brunschwig, B. S.; Creutz, C.; Sutin, N. *Chem. Soc. Rev.* **2002**, *31*, 168–184.
11. (a) Vahrenkamp, H.; GeiS, A.; Richardson, G.N. *J. Chem. Soc. Dalton Trans.* **1997**, 3643–3651; (b) Scandola, F.; Argazzi, R.; Bignozzi, C.; Chiorboli, C.; Indelli, M. T.; Rampi, M. A. *Coord. Chem. Rev.* **1993**, *125*, 283–292; (c) Scandola, F.; Bignozzi, C. A. "*Supramolecular Photochemistry*"; D. Reidel Publishing Company, 1987, pp. 121–133; (d) Vogler, A.; Osman, A. H.; Kunkely, H. *Coord. Chem. Rev.* **1985**, *64*, 159–173; (e) Watson, D. F.; Bocarsly, A. B. *Coord. Chem. Rev.* **2001**, *211*, 177–194; (f) Chang, C. C.; Pfennig, B.; Bocarsly, A. B. *Coord. Chem. Rev.* **2000**, *208*, 33–45; (g) Wu, Y.; Pfennig, B. F.; Sharp, S. L.; Ludwig, D. R.; Warren, C. J.; Vicenzi, E. P.; Bocarsly, A. B. *Coord. Chem. Rev.* **1997**, *159*, 245–255.
12. Richter-Addo, G. B.; Legzdins, P. "*Metal Nitrosyls*"; Oxford University Press: New York, 1992.
13. "*Methods in Nitric Oxide Research*"; Eds. Feelisch, M.; Stamler, J. S.; Wiley, 1996.
14. Averill, B. A. *Chem. Rev.* **1996**, *96*, 2951–2964.
15. Chen, P.; Meyer, T. J. *Chem. Rev.* **1998**, *98*, 1439.
16. Metelski, P. D.; Swaddle, T. W. *Inorg. Chem.* **1999**, *38*, 301–307.
17. Swinehart, J. H. *Coord. Chem. Rev.* **1967**, *2*, 385–402.
18. Westcott, B. L.; Enemark, J. L. "*Inorganic Electronic Structure and Spectroscopy, Vol. II: Applications and Case Studies*"; Eds. Solomon, E. I.; Lever, A. B. P.; J. Wiley & Sons, Inc., 1999, pp. 403–450.
19. Coppens, P.; Novozhilova, I.; Kovalevsky, A. *Chem. Rev.* **2002**, *102*, 861–884.

20. (a) Clarke, M. J.; Gaul, J. B. *Struct. Bonding (Berlin)* **1993**, *81*, 147–181; (b) Butler, A. R.; Glidewell, C. *Chem. Soc. Rev.* **1987**, *16*, 361–380; (c) Butler, A. R.; Megson, I. L. *Chem. Rev.* **2002**, *102*, 1155–1165.

21. Hoshino, M.; Laverman, L.; Ford, P. C. *Coord. Chem. Rev.* **1999**, *187*, 75–102.

22. (a) Wolak, M.; van Eldik, R. *Coord. Chem. Rev.* **2002**, *230*, 263–282; (b) Wanat, A.; Wolak, M.; Orzel, L.; Brindell, M.; van Eldik, R.; Stochel, G. *Coord. Chem. Rev.* **2002**, *229*, 37–49; (c) Laverman, L. E.; Wanat, A.; Oszajca, J.; Stochel, G.; Ford, P. C.; van Eldik, R. *J. Am. Chem. Soc.* **2001**, *121*, 285–293; (d) Schneppensieper, T.; Zahl, A.; van Eldik, R. *Angew. Chem. Int. Ed.* **2001**, *40*, 1678–1680.

23. Enemark, J. H.; Feltham, R. D. *Coord. Chem. Rev.* **1974**, *13*, 339–406.

24. Scheidt, W. R.; Ellison, M. K. *Acc. Chem. Res.* **1999**, *32*, 359–359.

25. Ford, P. C.; Lorkovic, I. M. *Chem. Rev.* **2002**, *102*, 993–1018.

26. Tfouni, E.; Krieger, M.; Mc Garvey, B. R.; Franco, D. W. *Coord. Chem. Rev.* **2003**, *236*, 57–69.

27. Ding, X. D.; Weichsel, Q.; Andersen, J. F.; Shokhireva, T. K.; Balfour, C.; Pierik, A. J.; Averill, B. A.; Montfort, W. R.; Walker, F. A. *J. Am. Chem. Soc.* **1999**, *121*, 128–138.

28. (a) Bottomley, F. "*Reactions of Coordinated Ligands*", Vol. II; Ed. Braterman, P. S. Plenum: New York, 1985, pp. 115–222; (b) Mc Cleverty, J. *Chem. Rev.* **1979**, *79*, 53–76.

29. Zollner, H.; Woike, Th.; Krasser, W.; Haussuehl, S. *Z. Kristallogr.* **1989**, *188*, 139.

30. (a) Chacón Villalba, M. E.; Guida, J. A.; Varetti, E. L.; Aymonino, P. J. *Spectrochim. Acta* **2001**, *A57*, 367–373; (b) Chacón Villalba, M. E.; Guida, J. A.; Varetti, E. L.; Aymonino, P. J. *Inorg. Chem.* **2003**, *42*, 2622–2627.

31. Morioka, Y.; Takeda, S.; Tomizawa, H.; Miki, E. *Chem. Phys. Lett.* **1998**, *292*, 625–630.

32. (a) Delley, B.; Schefer, J.; Woike, Th. *J. Chem. Phys.* **1997**, *107*, 10067–10074; (b) Gorelsky, S. I.; Lever, A. B. P. *Int. J. Quantum Chem.* **2000**, *80*, 636–645; (c) Boulet, P.; Buchs, M.; Chermette, H.; Daul, C.; Gilardoni, F.; Rogemond, F.; Schlapfer, C. W.; Weber, J. *J. Phys. Chem. A* **2001**, *105*, 8991–8998; (d) Boulet, P.; Buchs, M.; Chermette, H.; Daul, C.; Furet, E.; Gilardoni, F.; Rogemond, F.; Schlapfer, C. W.; Weber, J. *J. Phys. Chem. A* **2001**, *105*, 8999–9003.

33. Carducci, M. D.; Pressprich, M. R.; Coppens, P. *J. Am. Chem. Soc.* **1997**, *119*, 2669–2678.

34. Roncaroli, F.; Olabe, J. A.; van Eldik, R. *Inorg. Chem.* **2003**, *42*, 4179–4189.

35. Roncaroli, F.; Olabe, J. A.; van Eldik, R. *Inorg. Chem.* **2002**, *42*, 5417–5425.

36. (a) Nast, R.; Schmidt, J. *Angew. Chem. internat. Edit.* **1969**, *8*, 383; (b) van Voorst, J. D. W.; Hemmerich, P. *J. Chem. Phys.* **1966**, *45*, 3914–3918.

37. Wanner, M.; Scheiring, T.; Kaim, W.; Slep, L. D.; Baraldo, L. M.; Olabe, J. A.; Zalis, S.; Baerends, E. J. *Inorg. Chem.* **2001**, *40*, 5704–5707.

38. Langford, C. H.; Gray, H. B. "*Ligand Substitution Processes*"; W. A. Benjamin, Inc., 1965.

39. Waldhoer, E.; Kaim, W.; Olabe, J. A.; Slep, L. D.; Fiedler, J. *Inorg. Chem.* **1997**, *36*, 2969–2974.

40. (a) Cheney, R. P.; Simic, M. G.; Hoffman, M. Z.; Taub, I. A.; Asmus, K. D. *Inorg. Chem.* **1977**, *16*, 2187–2192; (b) Hankiewicz, E.; Stradowski, Cz.; Wolszczak, M. J. *Radioanal. Nucl. Chem. Lett.* **1986**, *105*, 291–302.

41. Toma, H. E.; Moroi, N. M.; Iha, N. Y. M. *An. Acad. brasil. Cienc.* **1982**, *54*, 315–323.

42. Legros, J. *J. Chim. Phys. Phys.-Chim. Biol.* **1964**, *61*, 909.

43. Toma, H. E.; Malin, J. M.; Giesbrecht, E. *Inorg. Chem.* **1973**, *12*, 2084.

44. Toma, H. E.; Malin, J. M. *Inorg. Chem.* **1973**, *12*, 2080.

45. Toma, H. E.; Batista, A. A.; Gray, H. B. *J. Am. Chem. Soc.* **1982**, *104*, 7509–7515.

46. (a) Toma, H. E.; Giesbrecht, E.; Malin, J. M.; Fluck, E. *Inorg. Chim. Acta* **1975**, *14*, 11; (b) Olabe, J. A.; Zerga, H. O.; Gentil, L. A. *J. Chem. Soc. Dalton Trans.* **1987**, 1267–1269.

47. (a) Bohle, D. S.; Hung, C. H. *J. Am. Chem. Soc.* **1995**, *117*, 9584–9585; (b) Bohle, D. S.; Debrunner, P.; Fitzgerald, J. P.; Hansert, B.; Hung, C. H.; Thomson, A. *J. Chem. Commun.* **1997**, 91–92.

48. (a) Butler, A. R.; Calsy-Harrison, A. M.; Glidewell, C. *Polyhedron* **1988**, *7*, 1197–1202; (b) Oszajca, J.; Stochel, G.; Wasiliewska, E.; Stasicka, Z.; Gryglewski, R. J.; Jakubowski, A.; Cieslik, K. *J. Inorg. Biochem.* **1998**, *69*, 121–127.

49. (a) Stochel, G.; van Eldik, R. *Inorg. Chim. Acta* **1991**, *190*, 55–59; (b) James, A. D.; Murray, R. S.; Higginson, W. C. E. *J. Chem. Soc. Dalton Trans.* **1974**, 1273–1278.

50. Hoshino, M.; Maeda, M.; Konishi, R.; Seki, H.; Ford, P. C. *J. Am. Chem. Soc.* **1996**, *118*, 5702–5707.

51. Roncaroli, F.; Ruggiero, M. E.; Franco, D. W.; Estiú, G. L.; Olabe, J. A. *Inorg. Chem.* **2002**, *41*, 5760–5769.

52. Wang, Y.; Averill, B. A. *J. Am. Chem. Soc.* **1996**, *118*, 3972–3973.

53. Silvestrini, M. C.; Tordi, M. G.; Musci, G.; Brunori, M. *J. Biol. Chem.* **1990**, *265*, 11783–11787.

54. Kim, C. H.; Hollocher, T. C. *J. Biol. Chem.* **1984**, *259*, 2092–2099.

55. (a) Swinehart, J. H.; Rock, P. A. *Inorg. Chem.* **1966**, *5*, 573–576; (b) Masek, J.; Wendt, H. *Inorg. Chim. Acta* **1969**, *3*, 455–458.

56. Wolfe, S. K.; Swinehart, J. H. *Inorg. Chem.* **1975**, *14*, 1049–1053.

57. (a) Masek, J.; Maslova, E. *Collection Czechoslov. Chem. Commun.* **1974**, *39*, 2141–2160; (b) Fiedler, J. *Collection Czechoslov. Chem. Commun.* **1993**, *58*, 461–473; (c) Bertolino, J. R.; Della Védova, C. O.; Sala, O. *Polyhedron* **1989**, *8*, 361–365; (d) Bowden, W. L.; Bonnar, P.; Brown, D. B.; Geiger, W. E. Jr. *Inorg. Chem.* **1977**, *16*, 41–43; (e) Carapuca, H. M.; Simao, J. E. J.; Fogg, A. G. *J. Electroanal. Chem.* **1998**, *455*, 93–105.

58. González Lebrero, M. C.; Scherlis, D. A.; Estiú, G. L.; Olabe, J. A.; Estrin, D. A. *Inorg. Chem.* **2001**, *40*, 4127–4133.

59. Baumann, F.; Kaim, W.; Baraldo, L. M.; Slep, L. D.; Olabe, J. A.; Fiedler, J. *Inorg. Chim. Acta* **1999**, *285*, 129–133.

60. Morando, P. J.; Borghi, E. B.; Schteingart, L. M.; Blesa, M. A. *J. Chem. Soc. Dalton Trans.* **1981**, 435–440.

61. (a) Wilson, R. D.; Ibers, J. A. *Inorg. Chem.* **1979**, *18*, 336–343; (b) Southern, J. S.; Hillhouse, G. L. *J. Am. Chem. Soc.* **1997**, *119*, 12406–12407; (c) Sellmann, D.; Gottschalk-Gaudig, T.; Hausinger, D.; Heinemann, F. W.; Hess, B. A. *Chem Eur. J.* **2001**, *7*, 2099–2103.

62. Gutiérrez, M. M.; Amorebieta, V. T.; Estiú, G. L.; Olabe, J. A. *J. Am. Chem. Soc.* **2002**, *124*, 10307–10319.

63. Alluisetti, G.; Almaraz, A. E.; Amorebieta, V. T.; Doctorovich, F. D.; Olabe, J. A. Work in progress.

64. Barley, M. H.; Takeuchi, K. J.; Meyer, T. J. *J. Am. Chem. Soc.* **1986**, *108*, 5876–5885.

65. Einsle, O.; Messerschmidt, A.; Huber, R.; Kroneck, P. M. H.; Neese, F. *J. Am. Chem. Soc.* **2002**, *124*, 11737–11745.

66. (a) Armor, J. N.; Hoffman, M. Z. *Inorg. Chem.* **1975**, *14*, 444–446; (b) Cheney, R. P.; Armor, J. N. *Inorg. Chem.* **1977**, *16*, 3338.

67. Olabe, J. A.; Estiú, G. L. *Inorg. Chem.* **2003**, *42*, 4873–4880.

68. Baraldo, L. M.; Bessega, M. S.; Rigotti, G. E.; Olabe, J. A. *Inorg. Chem.* **1994**, *33*, 5890–5896.

69. (a) Hendrich, M. P.; Logan, M.; Andersson, K. K.; Arciero, D. M.; Lipscomb, J. D.; Hooper, A. B. *J. Am. Chem. Soc.* **1994**, *116*, 11961–11968; (b) Hendrich, M. P.; Petasis, D.; Arciero, D. M.; Hooper, A. B. *J. Am. Chem. Soc.* **2001**, *123*, 2997–3005.

70. Forlano, P.; Parise, A. R.; Olabe, J. A. *Inorg. Chem.* **1998**, *37*, 6406–6407.

71. Burewicz, A.; Haim, A. *Inorg. Chem.* **1988**, *27*, 1611.

72. Roncaroli, F.; Baraldo, L. M.; Slep, L. D.; Olabe, J. A. *Inorg. Chem.* **2002**, *41*, 1930–1939.

73. Stanbury, D. M. *Adv. Inorg. Chem.* **1989**, *33*, 69–138.

74. Lunak, S.; Veprek-Siska, J. *Collection Czechoslov. Chem. Commun.* **1974**, *39*, 2719–2723.

75. Wolfe, S. K.; Andrade, C.; Swinehart, J. H. *Inorg. Chem.* **1974**, *13*, 2567–2572.

76. (a) Katz, N. E.; Blesa, M. A.; Aymonino, P. J. *J. Inorg. Nucl. Chem.* **1980**, *42*, 581–585; (b) Maciejowska, I.; Stasicka, Z.; Stochel, G.; van Eldik, R. *J. Chem. Soc. Dalton Trans.* **1999**, 3643–3649.

77. Johnson, M. D.; Wilkins, R. G. *Inorg. Chem.* **1984**, *23*, 231–235.

78. (a) Trogler, W. C. *Coord. Chem. Rev.* **1999**, *187*, 303–327; (b) Armor, J. N.; Taube, H. *J. Am. Chem. Soc.* **1969**, *91*, 6874–6876; (c) Bottomley, F.; Brooks, W. V. F. *Inorg. Chem.* **1977**, *16*, 501–502; (d) Tuan, D. F.; Hoffmann, R. *Inorg. Chem.* **1985**, *24*, 871–876.

79. Taube, H. *Pure Appl. Chem.* **1979**, *51*, 901–912.

80. Hidai, M.; Mizobe, Y. "*Reactions of Coordinated Ligands*", Vol. II; Ed. Braterman, P. S. Plenum Publ. Corp: New York, 1989, pp. 53–114.

81. Fomitchev, D. V.; Bagley, K. A.; Coppens, P. *J. Am. Chem. Soc.* **2000**, *122*, 532–533.

82. Douglas, P. G.; Feltham, R. D. *J. Am. Chem. Soc.* **1972**, *94*, 5254–5258.

83. (a) Dozsa, L.; Kormos, V.; Beck, M. T. *Inorg. Chimica Acta* **1984**, *82*, 69; (b) Butler, A. R.; Glidewell, C.; Reglinski, J.; Waddon, A. *J. Chem. Res. Synop.* **1984**, *9*, 279; (c) Casado, J.; Mosquera, M.; Rodríguez Prieto, M.F.; Vázquez Tato, J. *Ber. Bunsenges. Phys. Chem.* **1985**, *89*, 735; (d) Beck, M. T.; Kathó, A.; Dozsa, L. *Inorg. Chim. Acta* **1981**, *55*, L55.

84. Trápani, C.; Escola, N.; Doctorovich, F. *Organometallics* **2002**, *21*, 2021–2023.

85. Doctorovich, F.; Trápani, C. *Tetrahedron Lett.* **1999**, *40*, 4635–4638.

86. Doctorovich, F.; Escola, N.; Trápani, C.; Estrin, D. A.; González Lebrero, M. C.; Turjanski, A. G. *Organometallics* **2000**, *19*, 3810–3817.

87. Doctorovich, F.; Granara, M.; Di Salvo, F. *Transition Met. Chemistry* **2001**, *26*, 505–509.

88. (a) Akhtar, M. J.; Bonner, F. T.; Borer, A.; Cooke, I.; Hughes, M. N. *Inorg. Chem.* **1987**, *26*, 4379–4382; (b) Akhtar, M. J.; Bonner, F. T.; Hughes, M. N.; Lu, C. S.; Wallis, H. L.; Wimbledon, P. E. *Inorg. Chem.* **1987**, *26*, 2437; (c) Hughes, M. N.; Wimbledon, P. E. *J. Chem. Soc. Dalton Trans.* **1976**, 703.

89. Audrieth, L. F.; Ogg, B. A. "*The Chemistry of Hydrazine*"; J. Wiley & Sons: New York, 1951.

90. (a) Katz, N. E.; Olabe, J. A.; Aymonino, P. J. *J. Inorg. Nucl. Chem.* **1977**, *39*, 908–910; (b) Olabe, J. A.; Gentil, L. A. *Transition Metal Chem.* **1983**, *8*, 65–69.

91. Funai, I. A.; Blesa, M. A.; Olabe, J. A. *Polyhedron* **1989**, *8*, 419–426.

92. (a) Lehnert, N.; Wiesler, B. E.; Tuczek, F.; Hennige, A.; Sellmann, D. *J. Am. Chem. Soc.* **1997**, *119*, 8869–8878; (b) *ibid.* 1997, 119, 8879–8888, and refs. therein.

93. Keene, F. R. *Coord. Chem. Rev.* **1999**, *187*, 121–149.

94. da Costa Ferreira, A. M.; Toma, H. E. *J. Chem. Soc. Dalton Trans.* **1983**, 2051–2055.

95. Goto, M.; Takeshita, M.; Kanda, N.; Sakai, T.; Goedken, V. L. *Inorg. Chem.* **1985**, *24*, 582–587.

96. Toma, H. E.; da Costa Ferreira, A. M.; Murakami Iha, N. Y. *Nouv. J. Chim.* **1985**, *9*, 473–478.

97. Goedken, V. L. *J. Chem. Soc. Chem. Commun.* **1972**, 207.

  98. (a) Olabe, J. A.; Aymonino, P. J. *J. Inorg. Nucl. Chem.* **1974**, *36*, 1221–1226; (b) Blesa, M. A.; Olabe, J. A.; Aymonino, P. J. *J. Chem. Soc. Dalton Trans.* **1976**, 1196–1199.

  99. Katz, N. E.; Blesa, M. A.; Olabe, J. A.; Aymonino, P. J. *J. Chem. Soc. Dalton Trans.* **1978**, 1603–1606.

  100. Williams, P. A. M.; Aymonino, P. J. *Inorg. Chim. Acta* **1986**, *113*, 37–41.

  101. Herington, E. F. G. *J. Chem. Soc.* **1959**, *3633*, 72.

  102. Felix, F.; Ludi, A. *Inorg. Chim. Acta* **1977**, *24*, L-11.

  103. Bott, P. A.; Lott, K. A. K. *Inorg. Chim. Acta* **1986**, *111*, L33–L34.

  104. Wieghardt, K. *Adv. Inorg. Bioinorg. Mech.* **1984**, *3*, 213–274.

  105. Lunak, S.; Veprek-Siska, J. *Collection Czechoslov. Chem. Commun.* **1974**, *39*, 391–395.

  106. Lunak, S.; Veprek-Siska, J. *Collection Czechoslov. Chem. Commun.* **1974**, *39*, 41–48.

  107. Choi, I. K.; Liu, Y.; Wei, Z.; Ryan, M. D. *Inorg. Chem.* **1997**, *36*, 3113–3118.

  108. Banyai, I.; Dozsa, L.; Beck, M. T.; Gyemant, G. *J. Coord. Chem.* **1996**, *37*, 257–270.

  109. (a) Singh, J. *Biochimica et Biophysica Acta* **1973**, *333*, 28–36; (b) Allen, J. W. A.; Watmough, N. J.; Ferguson, S. J. *Nature Struct. Biol.* **2000**, *7*, 885–888.

  110. (a) Davies, G.; Garafalo, A. R. *Inorg. Chem.* **1976**, *15*, 1101–1106; (b) Bray, D. G.; Thompson, R. C. *Inorg. Chem.* **1994**, *33*, 905–909.

  111. Olabe, J. A. *et al.* Unpublished work.

  112. (a) Gmelins Handbuch der anorganischen Chemie, **1932**, *B59*, 903; (b) Baran, E. J.; Muller, A. *Z. Anorg. Allg. Chemie* **1969**, *B368*, 144–154.

  113. James, A. D.; Murray, R. S. *J. Chem. Soc. Dalton Trans.* **1977**, 319–321.

  114. Sulfab, Y. *Inorg. Chim. Acta* **1977**, *22*, 35–38.

  115. Kuehn, C. G.; Taube, H. *J. Am. Chem. Soc.* **1976**, *98*, 689–702.

  116. Kline, M. A.; Barley, M. H.; Meyer, T. J. *Inorg. Chem.* **1987**, *26*, 2197–2198.

  117. Lui, A. M.; Liang, W.; Soriano, A.; Cowan, J. A. *J. Am. Chem. Soc.* **1994**, *116*, 4531–4536.

  118. Szacilowski, K.; Stochel, G.; Stasicka, Z.; Kisch, H. *New J. Chem.* **1997**, *21*, 893–902.

  119. Schwane, J. D.; Ashby, M. T. *J. Am. Chem. Soc.* **2002**, *124*, 6822–6823.

  120. Szacilowski, K.; Wanat, A.; Barbieri, A.; Wasiliewska, E.; Witko, M.; Stochel, G.; Stasicka, Z. *New J. Chem.* **2002**, *26*, 1495–1502.

  121. Rock, P. A.; Swinehart, J. H. *Inorg. Chem.* **1966**, *5*, 1078–1079.

  122. Macartney, D. H.; McAuley, A. *J. Chem. Soc. Dalton Trans.* **1981**, 1780–1787.

  123. Oliveira, L. A. A.; Giesbrecht, E.; Toma, H. E. *J. Chem. Soc. Dalton Trans.* **1979**, 236–239.

  124. Vrachnou, E.; Gratzel, M.; McEvoy, A. J. *J. Electroanal. Chem.* **1989**, *258*, 193.

  125. (a) Yang, M.; Thompson, D. M.; Meyer, G. *J. Inorg. Chem.* **2002**, *41*, 1254–1262; (b) Blackbourn, R. L.; Johnson, C. S.; Hupp, J. T. *J. Am. Chem. Soc.* **1991**, *113*, 1060–1062; (c) Lu, H.; Proeskorn, J. N.; Hupp, J. T. *J. Am. Chem. Soc.* **1993**, *115*, 4927–4928; (d) Khoudiakov, M.; Parise, A. R.; Brunschwig, B. C. *J. Am. Chem. Soc.* **2003**, *125*, 4637–4642.

  126. Haim, A. ''*Adv. Chem. Ser.*''; American Chemical Society: Washington, USA, 1997, pp. 239–254, Chapter 14.

  127. Almaraz, A. E.; Gentil, L. A.; Baraldo, L. M.; Olabe, J. A. *Inorg. Chem.* **1996**, *35*, 7718–7727.

  128. Chen, M. H.; Lee, S.; Liu, S.; Yeh, A. *Inorg. Chem.* **1996**, *35*, 2627–2629.

  129. Ram, M. S.; Haim, A. *Inorg. Chem.* **1991**, *30*, 1319.

  130. Parise, A. R.; Baraldo, L. M.; Olabe, J. A. *Inorg. Chem.* **1996**, *35*, 5080–5086.

  131. Olabe, J. A.; Haim, A. *Inorg. Chem.* **1989**, *28*, 3277.

  132. Yeh, A.; Haim, A. *J. Am. Chem. Soc.* **1985**, *107*, 369.

  133. Nordmeyer, F.; Taube, H. *J. Am. Chem. Soc.* **1968**, *90*, 1162.